Magnetosphere-Ionosphere Coupling

N. Achilleos[1], L. C. Ray[2] and J. N. Yates[3]

1 Department of Physics and Astronomy, University College London;

2 Department of Physics, Lancaster University;

3 Arrival, Ltd., London, UK

February 9, 2021

1 Introduction

The interaction, or coupling, between a planet's magnetosphere and ionosphere (the ionised part of its upper atmosphere) involves the transport of energy and momentum between these two regions. This transport arises due to the fact that the planet's atmosphere is magnetically connected to its space environment. Magnetic field lines extend from the atmosphere into the surrounding magnetospheric volume. Electrical currents flow back and forth along these field lines in the intervening region, forming field-aligned currents (FACs). The current circuit 'closes' via ionospheric currents and distant magnetospheric currents which flow perpendicular to the magnetic field. The Lorentz volume force associated with a quasi-neutral plasma is $\boldsymbol{J} \times \boldsymbol{B}$, where the

respective symbols denote current density and magnetic field. The current flow which underpins magnetosphere-ionosphere (M-I) coupling thus transmits forces between these two regions.

While the 'current picture' is a useful one for exploring the 'microphysics' of M-I coupling, it is important to keep in mind that the M-I current system arises from the types of *plasma flow* which arise in the magnetosphere. These flows may be 'driven' by different sources of energy – for example, at the Earth the main driver is the interaction between the magnetosphere and the solar wind. On the other hand, Jupiter's dayside magnetosphere is typically two orders of magnitude larger than that of the Earth, with an interior plasma disc which rotates rapidly. As a result, the plasma flows in the Jovian system are dominated by internal rotation – specifically, the transport of the planet's angular momentum to the disc-like magnetosphere.

Regardless of the nature of the magnetospheric plasma flows (commonly known as the *convection* of plasma), the most intense field-aligned currents in the coupled M-I system arise at locations with the sharpest spatial gradients in the plasma flow velocity. Moreover, if these intense FACs are directed outwards from the planet's atmosphere, they are often supported at the microscopic level by energetic electrons 'raining' down along magnetic field lines into the atmosphere. These precipitating particles excite or ionise neutral molecules in the atmosphere, which radiate photons in characteristic wavebands when they de-excite or recombine. These photons form the *auroral emissions* of a magnetised planet, and the spectral characteristics and spatial morphology of these emissions are respective diagnostics of the precipitating particle energy distribution and the global pattern of magnetospheric plasma flow in the system.

Keeping these physical aspects of M-I coupling as our guide, we will explore in the following sections a few examples of this process at three different planets – the Earth, Jupiter and Saturn.

We choose to focus on these planets, as they provide useful illustrations of systems where M-I coupling is respectively associated with plasma flows driven by the solar wind interaction, the internal rotation of the planet, and a probable combination of these two 'extremes'.

2 The Earth

2.1 The Sun-Earth Connection

The Earth's aurorae are beautiful, coloured displays of light visible from high-latitude regions near the planet's magnetic poles (Figure 1). They are also a signature of the important influence of the Earth's space environment, or magnetosphere, upon the local structure of the atmosphere. The auroral emissions are generally produced by the precipitation – or 'rain' – of energetic particles, such as electrons and protons, from the Earth's space environment down onto the atmosphere. These particles can collide with neutral (and sometimes ionized) atmospheric species, transferring energy in the process, which is then radiated as photons when the excited atom / molecule relaxes back to a lower energy state. The wavelength of these auroral photons is an indicator of the radiating species (for example, the green colour in Figure 1 indicates a transition of atomic oxygen).

Particle precipitation in the auroral regions can also ionize neutral atoms and molecules in the atmosphere, contributing to the structure of the local ionosphere – the ionized species which co-exist with the neutral atmosphere. While local particle precipitation makes some contribution to ionization of the atmosphere in the auroral regions, the global ionosphere

of the Earth mainly arises from photoionization due to different wavebands of electromagnetic radiation from the Sun.

The lowest layer of the ionosphere is the D layer (altitude $\sim 60 - 90\,\mathrm{km}$**), arising from ionization of nitric oxide by ultraviolet (UV) Lyman-alpha (wavelength** $1216\,$**Å) photons. During times of high solar activity, ionization of molecular nitrogen and oxygen by hard X-rays (wavelength** $\lesssim 1\,\mathrm{nm}$**) may also occur. Next comes the E layer (**$90 - 150\,\mathrm{km}$**), where principal ionization is that of** O_2 **by soft X-rays (**$\sim 1 - 10\,\mathrm{nm}$**) and far UV radiation. The uppermost layer is the F layer (Appleton–Barnett layer,** $\sim 150 - 500\,\mathrm{km}$**). It has the highest electron density. Electrons here can be produced by extreme UV (**$10 - 100\,\mathrm{nm}$**) ionizing atomic oxygen. The F layer actually is one layer (F2) by night, but a secondary peak (F1) often also forms during the day. The comparatively small recombination rate for ions in F2 means that it is the only ionospheric layer with significant ionization during both day and night. The peak electron density in the F layer is typically of order** $\sim 10^6\,\mathrm{cm}^{-3}$**, situated around** $300\,\mathrm{km}$ **altitude.** ***Hargreaves*** **[1992] and** ***Rishbeth and Garriott*** **[1969] contain descriptions of the Earth's ionosphere, upper atmosphere and magnetosphere. Dynamics and structure of the upper atmospheres and ionospheres of the Earth and other solar system bodies, including auroral physics, are reviewed by, e.g.** ***Galand and Chakrabarti*** **[2002];** ***Gladstone et al.*** **[2002];** ***Waite Jr. and Lummerzheim*** **[2002];** ***Nagy and Cravens*** **[2002];** ***Bougher et al.*** **[2002];** ***Millward et al.*** **[2002];** ***Schunk*** **[2002].**

As we move higher in altitude, past the F layer's electron peak, we move into the topside ionosphere. From several hundred kilometres altitude upwards, we encounter the magnetosphere – a region extending over vast distances into space, where the dynamics of

charged particles in the plasma are strongly controlled by the internal magnetic field of the Earth and by the external field, generated by various forms of magnetospheric current. In the next two sections, we look at the types of plasma flows in the Earth's magnetosphere which arise from its interaction with the solar wind, and their relation to electric currents and auroral emissions. The theory of magnetospheric structure and formation by ? is an important foundation for contemporary magnetospheric physics.

2.2 Magnetic Reconnection: the Dungey Cycle

The terrestrial solar wind-magnetosphere interaction is schematically illustrated in **Figure 2a** (from *Baker et al.* [1987]). The diagram shows a noon-midnight 'cross section' of the system; the entire magnetosphere of the planet presents an obstacle to the solar wind plasma flowing towards it from the upstream region **(left-hand part of the diagram)**. One of the boundaries which is naturally produced by this flow-obstacle interaction is the magnetopause, a thin current layer which generally separates the plasma and magnetic field of the solar wind from those of the magnetosphere. Outside the magnetopause is the second boundary – the bow shock, which arises because the upstream solar wind moves at speeds in excess of the local magnetosonic speed **(magnetosonic waves in plasma being a type of analog here of sound waves through air)**. Sandwiched between these two boundaries is the plasma of the magnetosheath, which is produced when solar wind, upon moving through the bow shock, becomes strongly heated and compressed. The magnetosheath plasma flow is diverted around the magnetopause.

This separation between magnetosphere and solar wind plasma is not always enforced everywhere on the magnetopause – and it is this fact which is responsible for the magnetospheric plasma flows associated with M-I coupling. *Dungey* [1961] proposed that, for a strong southward orientation of the solar wind magnetic field (Interplanetary Magnetic Field (IMF)), **as shown in Figure 2a**, the magnetic fields of the solar wind and magnetosphere would be oppositely directed along the equatorial dayside magnetopause; and that this would lead to a merging or reconnection of the fields. ~~This process is illustrated in Figure ??b. The red curves represent open magnetic field lines which have resulted from the 'cross-linking' of neighbouring field lines, originally separated by the magnetopause. The left-most pair of open field lines have formed recently via dayside reconnection, and show the characteristic 'kink' arising from the large magnetic shear between the originally separated fields in the magnetosheath and magnetosphere.~~ **This dayside merging is illustrated by the magnetic field lines in 2a. We can picture IMF field lines as being frozen in to the flowing, collisionless plasma of the solar wind (consequence of Alfvén's theorem for perfectly conducting fluids). The leftmost field line has partly entered the subsolar magnetosheath - an area of slower plasma flow which thus causes the field line to bend as shown. As time proceeds, that part of the field line in the subsolar magnetosheath is carried all the way to the magnetopause where it merges or reconnects with a closed geomagnetic field line of opposite direction (labelled 1), so called because it has two footpoints on the Earth's surface. This merging forms two field lines, each with only one footpoint on the planet's surface. The most distant parts of these open field lines extend out into the ambient solar wind.**

Field lines labelled 2 in Figure 2a are examples of open field lines which continue to be

dragged downstream by the exterior solar wind flow, crossing over a high-latitude polar cap of open field as they do so. As shown, these open field lines get dragged further downstream into a region known as the magnetotail, formed by two lobes of sunward and antisunward field lines separated by a central plasma sheet (shaded region). The other labels in the diagram show a very disturbed plasma sheet structure on the nightside, which forms part of a larger cycle known as a substorm.

To put Figure 2a into context, we now refer to Figure 2b, which shows one of the best-known conceptual models of a magnetospheric substorm (after *Hones Jr.* [1984]). Panel 1 of this figure shows a quiescent magnetosphere, in which magnetotail lobe field lines (6,7) sink towards the midplane of the tail at the same time as their exterior portions continue to be dragged downstream by the solar wind. In this quiescent state, a distant neutral point (N) is formed in the magnetic field (typically of the order of 100 Earth radii downstream of the planet). This is shown in the diagram as an 'X'-shaped line, where a pair of open field lines flowing towards each other undergo reconnection and form: (i) A newly closed field line (planetward of the 'X') which snaps back towards the planet; and a newly formed field line which is accelerated away from the planet (downstream of the 'X') and rejoins the ambient solar wind.

In an idealized quiescent or steady state of this Dungey cycle – in which magnetic field lines (and their concomitant plasma) continuously move between open and closed topologies – the rate at which dayside merging converts closed magnetic flux to open would be balanced by the rate at which magnetotail reconnection converts open magnetic flux back to closed (indeed, a convenient dynamical unit for the system is a flux tube – comprising a

bundle, or tube, of magnetic field lines, either open or closed, along with the plasma carried along inside it).

In this relatively simple picture, the substorm sequence commences with a growth phase, where plasma, energy and magnetic flux are added to the widening magnetotail at a substantial rate – usually associated with a southward rotation of the IMF leading to enhanced dayside merging. This growth is also associated with a thinning of the tail plasma sheet and an enhancement of the current which it carries (e.g. *Akasofu and Snyder* [1972], *Hones Jr.* [1984], *Baker et al.* [1985], *Baker et al.* [1987], *Rostoker* [1999]). After a critical amount of plasma and energy have been stored in the magnetotail during the growth phase, a near-Earth magnetic neutral line (NENL) forms, as illustrated in Figure 2a and Figure 2b (panels 2,3,4). At this location, magnetic reconnection takes place until the thin plasma sheet is severed (panels 7,8). This event marks the substorm onset of the expansion phase, where a plasmoid - a structure containing plasma and magnetic flux now separated from the rest of the system - disconnects from the near-Earth plasma sheet and moves downstream at observed speeds of typically hundreds of $\mathrm{km/s}$. A recovery phase then ensues, allowing the extended magnetotail plasma sheet to be 'rebuilt' as plasma and magnetic field are continually added to the tail region, and the neutral line moves further downstream once more to its 'quiescent' position (panels 9,10).

Importantly, as shown in Figure 2a, the tail reconnection during substorms can energize plasma particles, some of which stream along newly closed magnetic field lines into the Earth's upper atmosphere, thus causing enhancement of auroral emissions. The auroral manifestation of substorms was described by early studies such as [*Akasofu and Chapman*,

1963; *Akasofu*, 1964] – indeed, Chapman suggested the 'substorm' terminology (a model of the substorm current sytem associated with magnetotail reconnection was described by [*McPherron*, 1972; *McPherron et al.*, 1973]). Substorms are usually several hours in duration; associated with local auroral enhancement and magnetotail reconnection; and often initiated by regular southward rotations of the IMF. Chains of substorms can also be elements of longer term events known as storms (e.g. [*Akasofu and Chapman*, 1963]). The earliest studies and records of geomagnetic storms include those of *Birkeland* [1918], *Moos* [1910], and *Chapman* [1918]. Storms are usually several days in duration; associated with global enhancement of auroral emissions; and commonly triggered by the passage of solar coronal mass ejections (often with prolonged southward IMF) around the magnetosphere. Fairfield and Cahill (1966) found that the southward component of the interplanetary magnetic field (IMF) played a crucial role in the development of geomagnetic storms.

In Figure 3, we show an example of one of the Earth's auroral signatures of a magnetospheric substorm, taken from *Wing et al.* [2013]. These maps of the averaged energy flux carried into the Earth's atmosphere by monoenergetic auroral electrons were derived by firstly identifying distinct substorm events using the ultraviolet auroral images from the Polar UVI and IMAGE satellite databases (these images contain emission bands of N_2 diagnostic of few-hundred-keV electrons, [*Liou et al.*, 1997; *Frey et al.*, 2004]). Subsequently, coincident precipitating particle data from the DMSP (Defence Meteorological Satellite Program, SSJ/4/5) satellite database were superposed, according to their epoch relative to the onset (zero time) of their associated substorm [*Newell et al.*, 2010].

We see that the auroral energy input flux derived from the data, for monoenergetic pre-

cipitating electron distributions, is concentrated mainly in the form of an arc, or partial oval, along the dusk-midnight sector (18:00–24:00 in the MLT (Magnetic Local Time) coordinates shown). It appears to reach a maximum at $\sim 15\,\mathrm{min}$ after substorm onset. The corresponding auroral electron power slowly increases $\sim 1.25\,\mathrm{hr}$ before onset, from typical values of $\sim 1\mathrm{GW}$ (integrated over both nightside hemispheres), and then increases quite dramatically at onset, up to $\sim 2\mathrm{GW}$ [*Wing et al.*, 2013]. This type of behaviour is likely associated with acceleration of electrons to form the monoenergetic distribution by magnetic-field-aligned electric fields, these being enhanced during substorm growth and onset. The auroral oval itself is usually near the boundary between open and closed magnetic field topologies (see section 2.3), and is also observed to expand in area during a well-defined growth phase (e.g. *Weimer et al.* [1992]) as the open magnetic flux stored in the system is increased by enhanced dayside magnetic merging.

However, this is just one example of a type of precipitating particle population which produces a specific type of aurora. Other morphological types of auroral emission (including ion aurora) can be similarly analyzed to yield information about other energy sources. For example, diffuse aurorae are associated with electron distributions covering a much broader range of energies. Those electrons with adequately magnetic-field-aligned motions lie in the loss cone of directions, and precipitate into the atmosphere; these are replenished by other electrons whose directions may be scattered into the loss cone through the interactions with specific types of electromagnetic wave (e.g. *Thorne* [2010]).

In the next section, we consider, in some more detail, currents in the Earth's ionosphere which arise from M-I coupling and their relationship to auroral emissions. In section 3.2,

we compare mechanisms of auroral particle acceleration at the Earth and at Jupiter.

An open field line has one 'end' connected to the planet, while its other ('open') end connects to the solar wind. The 'kink' in the field is associated with a strong magnetic curvature force that accelerates the plasma away from the reconnection site. In the collisionless plasma environment of the magnetosphere / solar wind, the magnetic field lines can be pictured as 'moving with' the plasma (the 'frozen-in' condition arising from Alfvén's theorem for perfectly conducting fluids). A convenient 'dynamical element' for visualising magnetospheric convection is the flux tube, consisting of a
Hence the subsequent motion of reconnected magnetic flux tubes, and their concomitant plasma, is also influenced by their 'open' end being carried downstream by the solar wind flow outside the magnetopause. As a result, the freshly opened flux tube is carried away from the reconnection site and moves polewards past the planetary terminator. As it moves further downstream into the nightside, it extends into a strongly radial or 'stretched' configuration, forming part of the *magnetotail*. As dayside reconnection continues to occur, more and more magnetic flux accumulates in the magnetotail region. To accommodate this growth, flux tubes on the night side sink towards a plane which separates lobes of oppositely directed magnetic field. These two lobes form from open flux tubes which have arrived in the tail via motion across the northward or southward polar region of the ionosphere (or 'polar cap', threaded by open magnetic flux). The nightside reconnection of flux tubes across the boundary plane between the tail lobes now converts two open magnetic field lines, one from each lobe, into a closed (blue) field line with both 'footpoints' attached to the planet; and a field line on the downstream side of the reconnection site with both ends open, which then becomes incorporated into the ambient solar wind flow. Again, strongly distended field lines arise following this closure of open flux, and

~~the accompanying magnetic curvature force accelerates plasma away from the reconnection site. The closed flux tubes arising from this process travel back towards the dayside magnetosphere, where they may again participate in dayside 'flux opening'. In a steady state picture of the Dungey cycle, the dayside flux opening rate is perfectly balanced by the nightside rate of closure. In reality, changes in the IMF orientation, and in magnetotail structure, lead to variability in these rates and they generally do not balance at any given time. The Dungey cycle thus describes the continual transi In addition, episodes of strong dayside reconnection and / or strong compressions of the magnetosphere can cause the formation of reconnection sites in the magnetotail which lie planetward of the 'steady-state' neutral point in the field. This type of configuration leads to events known as magnetospheric storms and substorms, involving dramatic reconfigurations of field and plasma. Storms are usually several days in duration; associated with global enhancement of auroral emissions; and commonly triggered by the passage of solar coronal mass ejections (with prolonged southward IMF) around the magnetosphere. Substorms are usually several hours in duration; associated with local auroral enhancement and magnetotail reconnection; and often initiated by regular southward rotations of the IMF.~~

2.3 Ionospheric Flows and Currents

To explore the ionospheric part of the M-I current system produced by Dungey cycle plasma flow, we commence with Figure 4 which shows schematic streamlines (black arrowed curves) depicting the typical motion of the northern ionospheric footpoint of flux tubes participating in this cycle. The central part of the diagram shows flux tube footpoints moving from the dayside

ionosphere (above the indicated solar terminator) across the polar cap. **As flux tubes cross the polar cap boundary (or OCB, open-closed field line boundary) at the top of the diagram, they also change their magnetic topology from closed to open (corresponding to the 'magnetospheric end' of the flux tube undergoing dayside merging, as described in section 2.2). The open flux tubes then move over the polar cap into the nightside, crossing the OCB again at lower latitudes – which now corresponds to flux closure in the magnetotail, transforming open field lines in that region into newly closed field lines (section 2.2).** ~~As flux tubes cross the polar cap boundary (or OCB, open-closed field line boundary) for the first time, they change configuration from 'single closed' to 'open pair', in response to ongoing dayside reconnection. The open flux tubes then move over the polar cap into the nightside, crossing the OCB again at lower latitudes – which corresponds to flux closure in the magnetotail, now transforming them into the northern portion of newly closed flux tubes.~~

The return flows in Figure 4 which lie outside the OCB, and which are directed from nightside to dayside, close the cross-polar-cap streamlines to form cycles or vortices. For a system with perfect magnetic field symmetry about the noon-midnight plane, and with entirely southward IMF, the Dungey vortices would also show perfect reflective symmetry about this plane. Figure 4 schematically depicts flows in the far more typical situation where there is a non-zero component of the IMF in the Y direction, perpendicular to the noon-midnight plane. Strong imbalances between the dayside and nightside reconnection rates also affect the morphology of the plasma flow vortices (see e.g. *Milan et al.* [2017] for more detail).

It is clear that the transpolar and return flows shown in Figure 4 show strong gradients in velocity across the polar cap boundary. This also leads to strong gradients in the convective elec-

tric field of the plasma ($\boldsymbol{E} = -\boldsymbol{v} \times \boldsymbol{B}$ for a perfectly conducting fluid, where $\boldsymbol{v}$ is bulk plasma velocity in the upper ionosphere). This convective electric field, to a first approximation, can be considered to be 'projected' along magnetic field lines (curves of constant electric potential) onto the main ionospheric conducting layers embedded in the atmosphere. In this collisional plasma regime, the electric field acts on charge carriers in the ionosphere and drives a system of currents, part of which is the Pedersen current that arises from ion-neutral collisions and which flows perpendicular to the local magnetic field (exact direction of the Pedersen current is influenced by local flows of the neutral atmosphere, which determine the electric field in the plasma rest frame). The green arrows in Figure 4 indicate the flow of Pedersen current, and illustrate strong gradients in Pedersen current density across the OCB.

The strong horizontal divergence in the Pedersen current must be closed in a steady state. Hence sheets of FAC arise in the vicinity of the OCB (blue circular symbols indicating upward or downward current flow); and equatorward of the OCB (red circular symbols). These are known respectively as the Region 1 and Region 2 current systems. **The upward-directed parts of each of these systems correspond to downward-moving (precipitating) electrons, and are thus co-located with the main ring of brightest auroral emission excited by these electrons as part of the terrestrial solar wind-magnetosphere interaction.**

Note that the $\boldsymbol{J} \times \boldsymbol{B}$ force exerted on the atmosphere by the Pedersen currents is directed antisunward across the polar cap, and is strongly aligned with the plasma return flows outside the polar cap. This is a symptom of the corresponding ion-neutral collisions 'dragging' the neutral atmosphere in the same general direction as the plasma flow in the collisionless upper ionosphere / magnetosphere. The Region 1 currents flow along the magnetic field over vast distances, and

connect the transpolar Pedersen currents to magnetopause currents. At the magnetopause, the associated $\boldsymbol{J} \times \boldsymbol{B}$ acts against the direction of solar wind flow. Hence, this part of the M-I current circuit ultimately transfers momentum from the ambient solar wind flow to the planet's atmosphere. The Region 2 currents flow at lower latitudes, and connect the atmospheric currents flowing equatorward of the OCB with the partial ring current in the magnetosphere. The Region 1, Region 2 and partial ring currents are sometimes referred to, collectively, as the 'convection circuit' (***Milan et al.* [2017], section 2.2**).

It is important to emphasise that the field-aligned current sheets associated with M-I coupling arise from plasma flow shears, which are, in turn, responsible for creating the shears in magnetic field that must be consistent with those currents, according to Ampère's Law. For example, in Figure 4 the flux tubes which travel across the polar cap can be pictured as being 'driven' by the solar wind flow outside the magnetopause (the 'dynamo') which effectively 'pulls' on the ionosphere-atmosphere medium (the 'load') via ion-neutral collisions. Hence, we expect the magnetic field to be tilted antisunward in this region of open magnetic flux. Similar reasoning leads us to expect a sunward tilt in the regions of return flow just outside the polar cap. Hence, a magnetic shear is set up across the OCB which must be consistent with the systems of FAC flowing between the ionosphere and magnetosphere.

There are additional indicated features in Figure 4 associated with the polar plasma flows and currents. These include Hall currents (orange arrows), part of which form circumpolar auroral electrojet currents; localised Region 0 FACs associated with plasma flow near the magnetospheric cusp **the high-latitude dayside region magnetically connected to locations where dayside merging is happening**; and the nightside wedge of current associated with magnetic

reconfiguration **in the magnetotail during a substorm (e.g. *McPherron* [1972]). For present purposes,** we will mainly focus on the larger-scale, steady-state current systems, acknowledging that additional localised currents and departures from the steady state are also present within general M-I coupling processes.

3 Jupiter

We now consider a M-I coupling system quite different in nature to that of the Earth. It is associated with the magnetosphere of the planet Jupiter, the largest and most strongly magnetised planet in the solar system. Two major differences between the Jovian and Terrestrial magnetospheres relevant for our discussion are:

- Jupiter's internal magnetic moment is approximately 18000 times as strong as the Earth's, leading to a much larger magnetosphere, with subsolar magnetopause location of typically 5.6 million km from planet centre, compared to about $640000\ \mathrm{km}$ for the terrestrial system.
- The main source of magnetospheric plasma for the Jovian system is an internal one – ionization of material ejected from the volcanic satellite Io. Io orbits Jupiter at a distance of $\sim 6\ \mathrm{R_J}$ (Jupiter radii, $1\ \mathrm{R_J} \approx 71500\ \mathrm{km}$).

Figure 5 illustrates some aspects of Jupiter's magnetosphere, with an inset of the terrestrial magnetosphere shown at the same scale for comparison. The main diagram shows a 'cut' through the Jovian system in the noon-midnight plane, with the yellow region indicating the outward transport of plasma from the Io plasma torus to form an enormous disc of plasma situated near

the equatorial plane (for more details about the physics of this radial plasma transport, see the review by *Achilleos et al.* [2015]; **and references in section 3.1**). The microscopic drift motions and collective gyrations of ions and electrons in the disc create a current sheet, whose azimuthal component carries of the order hundreds of MA, sufficient to distort the background dipole field of the planet into a more 'stretched', disc-like configuration.

3.1 Role of Rotation

One of the main forms of M-I couping in the Jovian system involves the transport of angular momentum between the planet and the plasma disc. A steady-state model of this process was described by *Hill* [1979] and is illustrated in Figure 6 from *Cowley and Bunce* [2001]. A useful way to picture the system is to consider the rotating planet as a source of angular momentum, which is magnetically connected to the magnetospheric plasma disc. Plasma produced near the Io neutral source forms a co-rotating torus anchored close to the magnetic equator. This plasma cannot build up indefinitely within the torus, and migrates radially outwards via a process known as flux tube interchange. Interchange is linked to a Rayleigh-Taylor type plasma instability, and is driven by the strong centrifugal force experienced by the plasma in a corotating frame of reference. Flux tubes of relatively cold, dense plasma continually 'trade places' with inward-moving tubes of hot, tenuous plasma from the outer magnetosphere. The tenuous flux tubes can then eventually 'refill' with Iogenic plasma, and thus the cycle repeats. The detailed physics of the process is a very active area of research (see e.g. **[*Gold*, 1959; *Melrose*, 1967; *Ioannidis and Brice*, 1971; *Hill*, 1976; *Southwood and Kivelson*, 1987; *Ferrière et al.*, 1999; *Ferrière and***

***André*, 2003]**).

In Hill's axisymmetric steady-state model, the plasma motion is modelled as a uniform radial outflow through a thin, planar disc. The total mass passing a given radial distance in the disc per unit time is denoted $\dot{M}$ and is equal to the plasma mass loading rate associated with the Io source. As plasma moves radially outwards, its tendency is to try and conserve its angular momentum, and thus rotate more slowly. Because it is magnetically connected to the planet, this 'slowing down' of the plasma produces azimuthal bendback in the magnetic field, which itself must be supported by radial currents in the disc plasma. These radial currents vary with distance, and thus must close via a system of field-aligned currents connecting them with the ionosphere. Equatorward ionospheric currents 'complete the circuit'. The net result is a transfer of angular momentum from planet to plasma, which maintains the plasma angular velocity at values above those which would otherwise prevail in the absence of this coupling.

This aspect is illustrated in Fig 7, which presents theoretical profiles of equatorial plasma azimuthal velocity according to Hill's theory for a pure dipole magnetic field. All of these profiles are determined by the co-rotational boundary condition at the inner radius (usually taken to be Io's orbit), and gradually become sub-corotational in the outer magnetosphere, where the finite ionospheric conductance and finite magnetic field strength can no longer supply adequate magnetic force to maintain corotation with the planet (or more correctly the planetary magnetic field). Note that the departure from corotation also occurs closer to the planet as the Iogenic mass loading rate $\dot{M}$ increases. Note also that profiles have considerably larger velocity than the corresponding Keplerian rotation curve, emphasising the dominance of M-I coupling over gravity in maintaining plasma rotation. Hill's theory provides an analytical estimate of the equatorial

distance L_0 (in planetary radii) at which the subcorotation starts to become significant ($\gtrsim 30\%$ departure from corotation):

$$L_0 = \left(\frac{\pi \Sigma_P B_J R_J^2}{\dot{M}} \right)^{1/4}.$$

This expression illustrates that L_0 decreases (i.e. coupling is less efficient) for decreasing ionospheric conductance Σ_P (which limits current density) and / or increasing plasma mass loading rate $\dot{M}$ (which produces a larger radial mass flux in the disc). An example of observations of the near-equatorial plasma velocity at Jupiter is shown in Figure 8. These velocities were determined from plasma observations by the *Galileo* spacecraft's Plasma Science instrument (PLS), and confirm the general tendency towards persistent sub-corotation with increasing distance.

3.2 Auroral Particle Acceleration

While this theoretical picture of coupling in a rotation-dominated system allows one to calculate the required FAC densities in the system, knowledge of the 'microphysics' of how those currents are carried relies on appeal to additional theoretical concepts. For example, earlier studies such as *Cowley and Bunce* [2001] employed the relation of *Knight* [1973] between the current density carried by precipitating electrons above the ionosphere and the field-aligned voltage $\Phi_{\parallel}$ typically required to accelerate those electrons, in order to allow a FAC density above the maximum value that can be carried in the absence of such acceleration. This type of process at the Earth is associated with auroral field-aligned current associated with $\Phi_{\parallel}$ of order a few kV. At Jupiter, application of this theory indicates that the auroral electrons must be accelerated to energies two orders of magnitude higher than typical magnetospheric energies. Since the typical thermal

electron energies are of order $\sim 1\,\mathrm{keV}$, the implied voltages are $\sim 100\,\mathrm{kV}$, thus accelerating auroral electrons to energies $\sim 100\,\mathrm{keV}$.

Subsequent analysis by *Ray et al.* [2009] showed that the linear approximation to Knight's relation, which had been used in previous studies of the coupled Jovian system, is not applicable in such rapidly rotating magnetospheres with an internal plasma source. Rapid rotation centrifugally confines heavy ions to near the equatorial plane, producing an ambipolar electric field that, in turn, restricts the mobility of the magnetospheric electrons. This effect, along with the gravitational confinement of the ionospheric plasma population, leads to a low plasma density at high latitudes. The local plasma population and magnetic field strength at high latitude determine the ensuing current-voltage relation. In Jupiter's middle magnetosphere, the hot electron population has an energy of $\sim 2.5\,\mathrm{keV}$ [*Scudder et al.*, 1981], and the mirror ratio in magnetic field strength between the top of the acceleration region (located at $\sim$ 2–3 $\mathrm{R_J}$ Jovicentric) and the planetary ionosphere (principal Pedersen conducting layer) has a value $R_x \sim 16$. Assuming the field-aligned potentials inferred from auroral observations of 30–200 kV, *Ray et al.* [2009] demonstrated that linear approximation of the Knight relation was not valid for such conditions. These authors thus used the full functional form of the Knight current-voltage relation [*Knight*, 1973], applied at the top of the acceleration region, rather than the magnetospheric equatorial plane. At $\sim 6\,\mathrm{R_J}$ (near Io orbit), this analysis indicated that applying the current–voltage relation at the magnetosphere, rather than high latitudes, could over-estimate the field-aligned current densities by about two orders of magnitude.

These types of studies thus illustrate the importance of accurately capturing the nature of particle acceleration mechanisms in order to infer the flux of energy delivered to the auroral

regions via particle precipitation. There is an abundant related literature based on combining *Hill* [1979]'s formalism with Jovian models of particle acceleration, non-dipolar magnetic fields, variable ionospheric conductance, and incorporating realistic hydrodynamic models of the neutral thermosphere and time-dependent flow models of the plasmasheet – (e.g. *Achilleos et al.* [2001]; *Nichols and Cowley* [2004]; *Cowley et al.* [2007]; *Smith and Aylward* [2009]; *Yates et al.* [2012]; *Ray et al.* [2010]; *Ray et al.* [2015]; *Yates et al.* [2018]).

More recently, plasma observations by the *Juno* spacecraft, currently orbiting Jupiter, have raised further questions about whether the 'field-aligned potential' acceleration mechanism is even the correct explanation for all instances of auroral emission excited in the neutral thermosphere / ionosphere by energetic particle precipitation from the magnetosphere. *Mauk et al.* [2018] examined electron energy distributions from the JADE (Jovian Auroral Distributions Experiment) acquired during low-altitude passes ($\sim 0.6 - 0.7\mathrm{R_J}$ above the clouds), very likely when the spacecraft was magnetically conjugate to the main auroral emissions. Many of these data indicated apparent transitions between electron energy spectra ($\lesssim 1\mathrm{MeV}$) with very different time-dependent characters. The first type of event was the usual 'inverted V' signature – electron energy constrained to a relatively small range, which shifts upwards with time to a maximum mean energy of typically hundreds of keV (the 'peak' of the inverted V) followed by a decline to lower energies once more. *Mauk et al.* [2018] noticed that near the peak energy of some of these events, the character of the spectrum changed to a population covering a much wider 'broadband' energy range, including a high-energy 'tail' indicating particle acceleration to much higher energies. Apart from this distinctive 'high-energy tail' for these Jovian events, this type of behaviour is similar to what is seen in the Earth's magnetosphere if observing spacecraft

move from a location inside the field-aligned potential drop (coherent acceleration mechanism) to a position below it in altitude. *Mauk et al.* [2018] interpreted such behaviour in Jupiter's electron energy distribution as a transition between the coherent acceleration, and a stochastic type of acceleration which produces significant particle flux over a wider range of energies.

The appearance of these stochastic or 'broadband' features could be associated with, for example, a kind of plasma instability which could arise when the FAC being 'drawn' by the magnetosphere-ionosphere coupling exceeds a certain limiting value. It also follows that for times / regions where currents are carried by stochastically accelerated electrons, the relationship between current density and downward-precipitating particle flux, as predicted by the relation of *Knight* [1973] is no longer valid. In fact, JADE observed one event with a downward accelerated proton inverted V, with inferred potentials of $300 - 400\,\mathrm{kV}$, occurring simultaneously with downward-accelerated broadband electrons with downward energy fluxes as high as $3000\,\mathrm{mW \cdot m^{-2}}$. This feature has no known counterpart from Earth auroral observations.

The theoretical analysis of *Saur et al.* [2018] demonstrated that, within a dipole shell of roughly $L \sim 30$ at Jupiter, the electron inertial length scale in the auroral region is the dominant scale in the plasma, suggesting that electron Landau damping of kinetic Alfvén waves can play an important role in converting field energy into auroral particle acceleration. This mechanism would be consistent with the broadband bidirectional electron distributions frequently observed by *Juno*. *Saur et al.* [2018] also hypothesised that, outside this region, ion cyclotron wave damping by heavy ions could play a role in heating magnetodisc plasma – whose monotonically increasing temperature with distance in the magnetosphere lacks a definitive explanation (e.g. *Bagenal and Delamere* [2011]). What remains clear is that there are many details of the physics

of M-I coupling and associated auroral acceleration at Jupiter that are yet to be definitively described.

In the related context of auroral particle acceleration at the Earth, the much earlier theoretical work of *Lysak and Song* [2003] demonstrated that the broadband type of acceleration was not consistent with a purely electrostatic potential drop and suggested a wave heating of auroral electrons. These authors pointed out that Alfvén waves had been observed on Earth auroral field lines carrying sufficient Poynting flux for this mechanism. Their calculations, based on the linear kinetic theory of Alfvén waves, indicated that Landau damping of these waves can efficiently convert this Poynting flux into field-aligned kinetic energy of electrons. At comparatively low altitudes along auroral field lines, the gradient in the Alfvén speed becomes significant, thus requiring a nonlocal description. *Lysak and Song* [2003] described a nonlocal theory based on a simplified model of the ionospheric Alfvén resonator (IAR). For a given density of FAC, they demonstrated that the efficiency of the wave–particle interaction increases with the ratio of the thermal electron velocity to the Alfvén speed at high altitudes. Their calculations indicated that wave acceleration of electrons should occur at and above the altitude where the quasi-static potential drops (associated with coherent acceleration) form.

We have mainly focused in this section on the M-I coupling in 'middle magnetosphere' of Jupiter, since it is associated with the brightest auroral emissions, also known as the 'main emission' - oval-shaped loci of persistent emission which surround the planet's magnetic poles and seem to be carried around by the rotation of the planet itself, strong evidence for an internally generated auroral current system. There also exist rapidly-varying auroral features poleward of the main emission whose physical origin remains undefined. Future analyses of auroral and in

situ observations by *Juno* should help elucidate these features. Other types of transient aurorae arise due to, for example, flux tube interchange events in the middle magnetosphere, which magnetically map to the ionospheric region between the locus of the Io 'spot' aurora and the main emission (see Figure 9 for examples of different auroral features at Jupiter). The Io spot-like aurora is an important signature of M-I coupling, and is thus briefly described in the following subsection.

3.3 Io-Jupiter Interaction

The Io-Jupiter interaction has no analog at the Earth. Io has an electrically conducting ionosphere, which is exposed to the ambient Jovian magnetic field and corotating plasma torus that sweep past it at a speed $\sim 56\,\mathrm{km}\cdot\mathrm{s}^{-1}$. Early observations of the decametric radio emission (DAM) inspired models involving a continuous electric current linking the Jovian ionosphere with Io acting as a unipolar inductor with potential difference $\sim 400\,\mathrm{kV}$ induced across its diameter (e.g. *Piddington and Drake* [1968]; *Goldreich and Lynden-Bell* [1969]).

Near-Io observations by *Voyager 1* detected a magnetic perturbation associated with a $\sim 3\,\mathrm{MA}$ current along the Io flux tube (IFT) [*Acuña et al.*, 1981]. This FAC would be carried by Alfvén waves continually launching and propagating at a speed determined by the local plasma density [*Belcher*, 1987]. Since the torus is anchored close to Jupiter's rotating, tilted dipole equator, it moves north and south of Io as rotation proceeds, causing a $\sim 20\%$ modulation in local magnetic field strength, and a variation in the current path.

In this picture, the motion of Io, a conducting body, through Jovian magnetic field is anal-

ogous to an electrodynamic generator, and produces electron energisation and precipitation towards the planet. This, in turn, excites ultraviolet and infrared auroral emissions at or near Io's magnetic flux tube footprint. At radio frequencies, the emission from the Io-induced source (the 'Io-DAM') spans the range $\sim$ 1–40 MHz. Electrons accelerated by the interaction can produce strongly-beamed radiation as they move within the magnetic field of Jupiter (e.g. *Le Quéau* [1988]; *Queinnec and Zarka* [1998]).

The anti-correlation between Io-DAM occurrence and the brightness of near-IFT IR and UV auroral emission is an important diagnostic of electron dynamics in the system. *Zarka et al.* [1996]'s interpretation involved near-Io Alfvén waves accelerating electrons which then precipitate towards the planet. A variable fraction of these mirror before they reach Jupiter's ionosphere, due to the continual change in magnetic field strength near the IFT footprint. This reflected component exhibits a loss-cone distribution and can thus produce radio emission via the cyclotron maser instability. Similarly, an anti-correlated fraction of the precipitating electrons reach the ionosphere and excite UV / IR auroral emissions. The Io-DAM power radiated is typically 10^9–10^{10} W. The IR and UV spots near the IFT magnetic footprints on Jupiter's ionosphere correspond to radiated powers of $\sim 3 - 10 \times 10^{10}$ W and $\sim 2 - 10 \times 10^{10}$ W [*Prangé et al.*, 1996; *Satoh and Connerney*, 1999; *Clarke et al.*, 2002].

High-resolution images of the Io-related auroral UV emissions often reveal a main spot approximately magnetically conjugate with the Io body, accompanied by local emission 'upstream' of this location, and one or more spots 'downstream'. The interpretation of such patterns can reveal much about the complex paths of Alfvénic disturbances propagating between Io and Jupiter, including 'multiple wave bounces' arising from partial reflection and transmission at the bound-

aries of the plasma torus (e.g. *Bonfond* [2013]).

3.4 Role of Magnetic Reconnection

Finally, we note some relevant aspects concerning the role of magnetic reconnection for M-I coupling at Jupiter. *Vasyliūnas* [1983] described 'reconnection' on a single, closed field line which becomes strongly radially distended as it rotates into the dusk-midnight local time sectors. If the flux tube is adequately mass-loaded with plasma, the thin current sheet which separates its northern (radially outward) and southern (radially inward) field line segments will become disrupted. This type of field topology, as discussed in Section 2, promotes reconnection which, in this case, leads to the detachment of the 'tip' of the flux tube, which forms an individual plasmoid that continues moving downstream, eventually becoming incorporated with ambient solar wind plasma. This process is quite different to the nightside reconnection of the Dungey cycle (Section 2), which forms a closed flux tube from two previously open ones. The relative importance of the Vasyliūnas and Dungey cycles in Jupiter's magnetospheric dynamics is a subject of debate (e.g. *Cowley et al.* [2003], *Kivelson and Southwood* [2005], *McComas and Bagenal* [2007], *Southwood and Chané* [2016]).

Desroche et al. [2012] analysed expected field and plasma conditions at the Jovian magnetopause for a relatively expanded system. They concluded that reconnection would be inhibited on the dawn flank due to the large-shear flows in this region, regardless of magnetopause shape or IMF orientation. The presence of a hot magnetospheric plasma population in the magnetosphere could inhibit reconnection over much of the magnetopause area (influence of diamagnetic

drift), except when the neighbouring magnetic fields were antiparallel. Most of the dawn flank of the magnetopause was demonstrated to be Kelvin-Helmholtz (KH) unstable, regardless of magnetopause asymmetry; this was consistent with a result of the related study by *Masters* [2017], which also showed that the structure of the KH-unstable dawn region was less sensitive to changing conditions than were the predicted locations of reconnection across the magnetopause.

In this context, is also important to note that the term 'lobe', as commonly used for the Jovian magnetosphere, does not necessarily refer to regions of open magnetic flux, as it usually does for the terrestrial magnetotail (Section 2.2). The relatively cool plasma population at Jupiter is centrifugally confined and exists in the form of a vast, near-equatorial plasma sheet at all local times (as described earlier in this Section) which co-exists with the magnetotail plasma / current sheet. The regions outside several plasma scale heights from the local plane of these confined plasma sheets are comparatively lacking in plasma and can be considered lobe regions from that point of view – even when situated on closed magnetic field lines.

4 Saturn

A large body of observational evidence supports the notion that M-I coupling at Saturn is 'Earth-like', from the point of view of explaining auroral morphology, and 'Jupiter-like', in terms of describing rotationally-dominant plasma flows. The *Cassini* mission also uncovered evidence for a localised, rotating system of currents in Saturn's magnetosphere which imposes ubiquitous quasi-periodic oscillations in the observed magnetic field and plasma parameters. This periodicity can plausibly be connected to an atmospheric source, whose ultimate source of energy

remains, as yet, unclear. We explore these aspects further in the following subsections.

4.1 Aurora

The obervations of Saturn's southern aurora presented and analysed by *Badman et al.* [2005] were particularly important in elucidating auroral physics. The relevant sequence of ultraviolet auroral images, presented in Figure 10, encompassed the time when a solar wind compression region observed in situ, upstream of Saturn, by the *Cassini* spacecraft, had been predicted to reach the planet's magnetosphere. More specifically, the images from HST Visits 10, 11 and 12 show the most strongly disturbed auroral emissions compared to the first two images in the sequence, which are more typical of the quiescent auroral state at Saturn. The nature of the auroral disturbance involves a clear brightening of the emissions, combined with the retreat of their poleward boundary to higher latitudes, thus transforming the quiescent 'oval' or 'ring' of emission into an aurora which 'fills in' much of the dawn local time sector of the polar atmosphere.

The origin of this auroral event was indicated by in situ observations acquired by *Cassini* in the solar wind upstream of Saturn - particularly those acquired ~ 18 hours earlier than the Visits 10-12 observations. This time difference was a good estimate of the time required for solar wind plasma to propagate from *Cassini*'s location to Saturn's magnetosphere, plus the time required for photons from any auroral events triggered to reach the HST. The relevant in situ magnetic field and plasma data indicated a compression region in which the dynamic pressure of the solar wind plasma and the magnitude of the IMF increased by about an order of magnitude, and in which the orientation of the IMF underwent a significant rotation indicating a traversal of the heliospheric

current sheet. By using an empirical formula (adapted from terrestrial studies) for estimating the corresponding voltage associated with magnetic reconnection, *Badman et al.* [2005] illustrated that this compression event would likely drive a strong episode of magnetospheric compression and dayside reconnection, once it reached Saturn's magnetosphere. The disturbed auroral observations showed responses qualitatively similar to those of the terrestrial magnetosphere to such a solar wind compression. For example, the Visit 11 image shows the 'dawn auroral filling' that would be expected to follow a compression-induced episode of magnetotail reconnection, with the auroral emissions excited by energetic electrons streaming from active reconnection sites in the nightside magnetosphere, along newly-closed magnetic field lines now connecting to the dawnside ionosphere **(in situ field and particle signatures confirming reconnection in Saturn's magnetotail were analysed in early** *Cassini* **studies such as *Jackman et al.* [2007],*Hill et al.* [2008])**. The Visit 12 image shows a subsequent equatorward expansion of the auroral emissions, consistent with ongoing dayside reconnection expanding the area of open magnetic flux in the system – assuming that the brightest persistent emissions, as for the case of the Earth, demarcate a boundary at or near the OCB.

Analysis of magnetospheric data acquired by *Cassini*, combined with remote observations and conceptual models of ionospheric plasma flow, supported the hypothesis that Saturn's main auroral emissions were magnetically conjugate to a layer of closed field lines in the outer magnetosphere, close to the actual OCB. In this picture, the OCB, located typically near 15° colatitude, is also the location of a strong plasma flow shear, mainly due to a change in the inferred rotational velocity of the plasma between the closed and open regions of magnetic flux (e.g. *Stallard et al.* [2004]; *Cowley et al.* [2008]; *Bunce* [2013] and references therein). While such studies

have indicated an 'Earth-like' origin for the main auroral emissions at Saturn, there has also been evidence for the presence of fainter, equatorward auroral emissions (infrared radiation from ionospheric H_3^+ molecular ions) which have been interpreted as the Kronian analog of Jupiter's corotation-related aurora [*Stallard et al.*, 2008].

A more recent study of auroral images of Saturn, using a comprehensive database, has been conducted by *Bader et al.* [2019]. This study has revised the interpretation of the main ring of steady auroral emission as arising from subcorotation – specifically flow shear between middle and outer magnetospheric plasma layers – upon which are superposed two rotating current systems associated with near-planetary period oscillations in the magnetosphere (see Section 4.2). Important revelations arising from this work were: (i) The main emission arising from subcorotation has no significant asymmetry in local time, and is thus not affected by any putative Dungey cycle activity; (ii) The main emission is typically overpowered by large, bright auroral 'patches' which are a likely consequence of magnetotail reconnection processes. *Bader et al.* [2020] examined unique high-resolution auroral data from *Cassini* during the final 'Grand Finale' orbits, which brought the spacecraft closer to the planet than previous mission segments. This analysis revealed the main arc of auroral emission to be variable between smooth and rippled appearance, suggestive of a transition between a quiet and disturbed magnetosphere. A fainter, more diffuse emission also typically exists equatorward of the main emission. This fainter component is consistent with generation by a population of hot electrons, residing in the inner ring current region, being wave-scattered into their loss cone – as concluded by *Grodent et al.* [2010] from a much earlier study which employed UV auroral images acquired by the HST Imaging Spectrograph (STIS).

4.2 Periodic Phenomena

Periodic modulation of Saturn's auroral kilometric radiation (SKR) was observed during the *Voyager 1* mission and used to infer a planetary rotation period of 10h 39m 24s $\pm$ 7s [*Desch and Kaiser*, 1981]. With the arrival of *Cassini* 24 years later, a slightly different period of 10h 45min 45s $\pm$ 36s was determined [*Gurnett et al.*, 2005; *Kurth et al.*, 2008]. As well as this 'drift' of the underlying period, there also appears to be a difference in the periods between the northern hemisphere ($\sim$ 10.6 hrs) and the southern hemisphere at ($\sim$ 10.8 hrs) [*Gurnett et al.*, 2009]. The difference in these two rotation rates appeared to converge about seven months after Saturn's equinox in 2009.

This periodicity is a surprise, since the planet's internal magnetic field is highly aligned with its rotational axis (e.g. *Cao et al.* [2011]). The period drift suggests that it is not due to planetary rotation alone. The different northern and southern periods further complicate any potential explanation of their physical origin. The same quasi-periodic modulation has been observed in many of the properties of the Kronian magnetosphere, including the magnetic field [*Espinosa and Dougherty*, 2000; *Giampieri et al.*, 2006; *Cowley and Provan*, 2017], low-energy plasma [*Gurnett et al.*, 2007], energetic charged particles [*Carbary et al.*, 2007], energetic neutral atoms [*Paranicas et al.*, 2005; *Carbary et al.*, 2008], and the position of the magnetopause [*Clarke et al.*, 2010]; see also the review by *Carbary and Mitchell* [2013]. Substantial work has also been done on characterising the global near-planetary-period oscillations (PPOs) in the magnetic field and using them to infer the behaviour of the amplitude and phase with position and time (e.g. *Andrews et al.* [2012]; *Cowley and Provan* [2017] and references therein). An interesting

consequence of this characterisation, which is consistent with observations by *Cassini*, is that the phase difference between the northern and southern oscillations determines the detailed nature of the periodic modulation in the altitude (with respect to the rotational equator) and thickness of the plasma sheet (e.g. *Thomsen et al.* [2017]; *Sorba et al.* [2018]; *Ramer et al.* [2017]). The two 'extremes' of this modulation are the 'flapping' mode involving only a modulation in plasma sheet altitude; and the 'breathing mode' involving only a modulation in sheet thickness.

An important strand of modelling work interprets the PPOs as the consequence of a form of M-I coupling which involves two distinct rotating current systems ('northern' and 'southern') driven by localised vortical flows in the planet's high-latitude ionosphere. *Smith and Achilleos* [2012] used a global circulation model of Saturn's thermosphere to demonstrate that the necessary vortical flows would arise from a source of longitude-dependent heating near auroral latitudes, which didn't necessarily have to be continually active. Their results were in qualitative agreement with the phase relations of the observed PPO magnetic oscillations, although quantitative agreement was lacking. The related study by *Jia et al.* [2012] acquired quantitative agreement with plasma and magnetic oscillations by employing a sophisticated model of the Kronian magnetosphere, driven by a prescribed ionospheric flow as an interior 'boundary condition'. Such studies have provided insight into this additional manifestation of M-I coupling, although they do not provide a first-principles explanation for the ultimate source of energy for the required atmospheric vortical flows. Additional models, based on atmospheric wave modes and magnetospheric plasma instability associated with Saturn's polar cap region, have been respectively described by *Smith et al.* [2016] and *Southwood and Cowley* [2014].

The observed influence of this PPO-related coupling on auroral emissions has been described

by *Nichols et al.* [2008], who analysed auroral images of Saturn to reveal a systematic periodic 'wobbling' of the planet's main auroral oval. The related perturbations introduced by the PPO-related current systems onto the subcorotation-related auroral currents in Saturn's magnetosphere (flow shear at or near the OCB) were analysed by *Hunt et al.* [2018, 2020].

5 Radio Emissions

We have discussed radio emissions as a signature of M-I coupling processes in the context of the Io-Jupiter interaction (Section 3.3) and the periodic phenomena of Saturn's magnetosphere (Section 4.2). In a broader context, radio emissions are produced by a variety of M-I coupling mechanisms. In auroral acceleration regions at the Earth, for example, the electron cyclotron maser instability generates radio emission when the local plasma frequency approaches the gyrofrequency (e.g. *Ergun et al.* [2000]; *Melrose and Dulk* [1982]; *Wu and Lee* [1979]).

The Saturn kilometric radiation (SKR) exhibits similar periodic behaviour to the magnetic field perturbations, which can be disrupted during strong episodes of magnetospheric compression [*Badman et al.*, 2008]. SKR can also provide information on plasma injections, possibly associated with magnetotail reconnection [*Lamy et al.*, 2013]. At Jupiter, apart from the Io-Jupiter interaction, the coupling between the planet and the middle magnetosphere is associated with radio emissions spanning the decametre-to-kilometre range (e.g. *Zarka* [1998]). Observations from *Juno* suggest that the sources of these emissions are likely to be widespread throughout the Jovian system [*Kurth et al.*, 2017].

Planet / Approx. Rotation Period τ (h)	Relative Magnetic Moment / Approx. Equatorial Field (nT)	Solar Wind Travel Time^{+} T_S (Bow to Planet, min)	Average Auroral Brightness / Input Power^{x}	Global Joule Heating	Ratio τ/T_S
Earth / 24	1 / 30000	2	1-100 kR (1-100 GW)	10-100 GW[1]	720
Jupiter / 10	20000 / 400000	200	10-1000 kR (few $\times$ 10 TW)	$\sim$ 200 TW[2]	3
Saturn / 11	580 / 20000	40	1-100 kR (0.1-1 TW)	$\sim$ 10 TW[3]	16.5

Table 1: Comparison of planetary and magnetospheric parameters for the three planets considered herein. Data were obtained / derived from the table of *Clarke* [2013], except for: [1]*Olsson et al.* [2004]; [2]*Yates et al.* [2020]; [3]*Cowley et al.* [2004]. $^{+}$ Calculation assumes a solar wind speed $500\,\mathrm{km}\cdot\mathrm{s}^{-1}$. ^{x} Conversion of 10% of input energy into auroral emission has been assumed.

6 Summary and Conclusions

We commence this summary with reference to Table 1, which compares fundamental magnetospheric, ionospheric and auroral parameters – which all play a role in M-I coupling and its consequences – at the three different planetary environments we have considered. We note that Jupiter, the most strongly magnetised planet with the largest magnetosphere, also has the brightest polar auroral emissions, and the largest integrated energy input to the atmosphere (carried by precipitating particles) required to produce those emissions. The typical auroral brightness (photon flux per unit area per unit time from the emitting layer) for the Earth and Saturn are similar, although Saturn, being the larger planet, has an associated energy input which is an order of magnitude (or more) greater. For all three planets, the global power dissipated by the atmospheric Joule heating (from ionospheric currents) is comparable in magnitude, or greater than, the auroral energy input (although for the gas giants, the Joule heating estimates rely on model-dependent assumptions regarding ionospheric conductance).

The column indicating the ratio of the planetary rotation period to the solar wind travel time (time required for ambient solar wind to travel from bow shock position to planetary terminator plane) shows that this quantity spans almost three orders of magnitude between the three planets. At one extreme, the Earth has a very slow rotation compared to the solar wind flow time, consistent with the solar wind interaction being the principal determinant of plasma flows in the outer magnetosphere. At the other extreme, Jupiter's rotation period is comparable to the solar wind flow time, consistent with rotation-dominated flows in the Jovian system, as we have described in this overview.

The discussions related to M-I coupling in the previous sections have considered this process within the space environments of three different planets. Despite the vast differences in the magnetic field strengths and plasma flow patterns in the magnetospheres we have considered, the following common themes related to M-I coupling can be discerned.

- M-I coupling, by definition, involves the transfer of energy and momentum between the planet and the plasma in its magnetosphere. This process may involve the communication of the momentum in the solar wind to the planet's polar ionosphere, and / or the transport of angular momentum between the planet and a rapidly-rotating magnetosphere. The transport of momentum must occur over vast distances within the magnetosphere (typically tens of planetary radii or greater).

- The transport of momentum and energy is mediated by systems of magnetic field-aligned currents which flow between the planet and the relevant magnetospheric regions, which in the steady state are closed by ionospheric currents and 'cross-field' magnetospheric

currents.

- The most intense field-aligned currents are usually conjugate to regions of strong plasma flow shear, and are usually associated with the brightest auroral emissions excited in the planetary atmosphere by the precipitation of energetic particles from the magnetosphere.

- The microscopic nature of auroral currents and the required acceleration of current-carrying particles remains to be fully quantified and described, particularly for the giant planets. Recent observations from spacecraft such as *Juno* indicate that at least two different modes of particle acceleration prevail – respectively associated with the formation of magnetic field-aligned electric potentials, and the stochastic acceleration of particles via some kind of plasma instability or wave-particle interaction.

- Many types of auroral emission still lack a definitive explanation, and some of these may require a better understanding of the complex coupling 'feedback' between the planet's atmosphere and magnetosphere, in the context of departures from the steady-state picture.

Figure 1: Image of aurora borealis (northern lights) in the night sky. The mainly green emission is from excited atomic oxygen, while the blue emission is from nitrogen. The rapid decrease of atomic oxygen below $\sim 100\,\mathrm{km}$ is responsible for the fading of the lower edges of the 'curtains'. (Image Credit: Jerry Magnum Porsbjer, Wikimedia Commons under the Creative Commons license https://creativecommons.org/licenses/by-sa/3.0/deed.en)

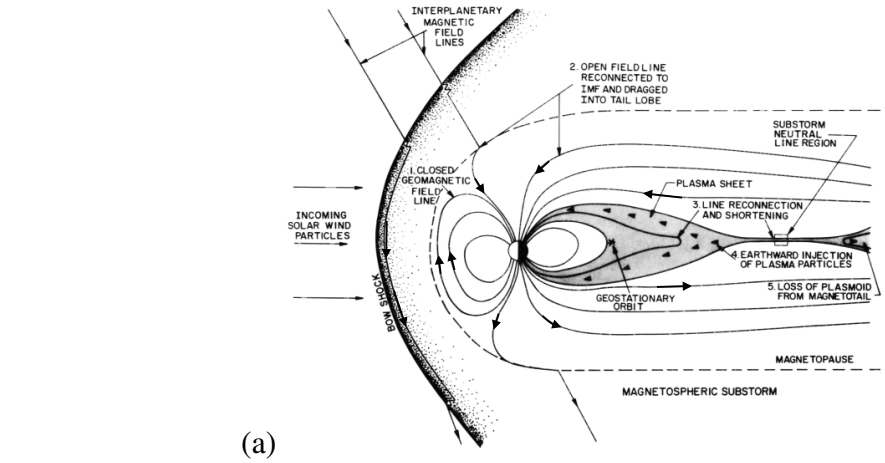

(a)

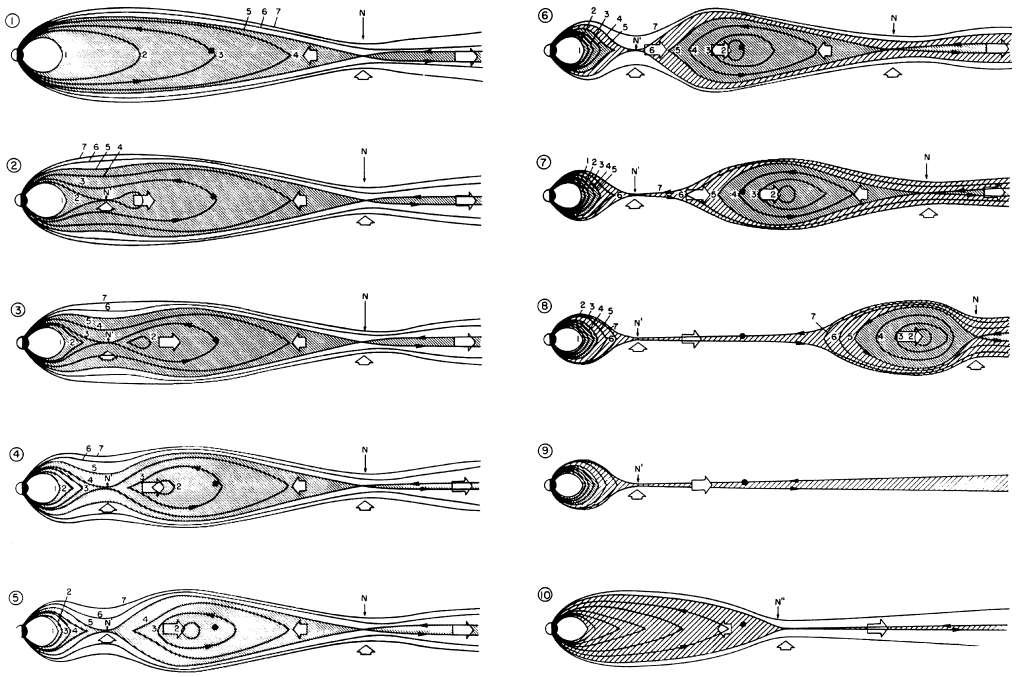

(b)

Figure 2: (a) Schematic of the noon-midnight terrestrial magnetosphere, where the nightside magnetotail illustrates expansion onset during a substorm (from *Baker et al.* [1987]); (b) Phases of a substorm (see text) after *Hones Jr.* [1984]. Individual field lines are labelled in all the diagrams of the magnetotail region, which shows the development of a near-Earth neutral line during the growth phase (panels 1–6). Thick white arrows indicate plasma flow.

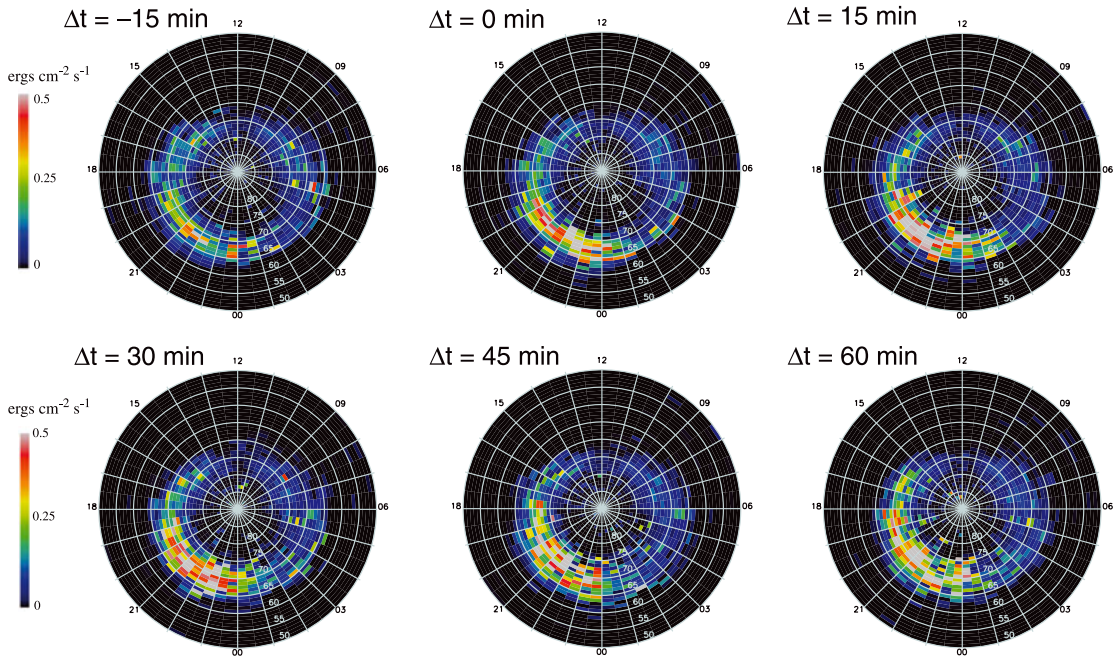

Figure 3: From *Wing et al.* [2013] (only part of the original figure is shown here, for clarity): Hemispherical maps of auroral input energy flux at the Earth for monoenergetic auroral electrons, derived from satellite-based ultraviolet imaging of auroral emissions and in situ particle data. The colour scale shows averaged energy flux inferred from the data over the combined northern and southern polar regions, organized according to epoch relative to substorm onset (time zero). The maps are produced by epoch superposition of individual image sequences coincident with substorm events.

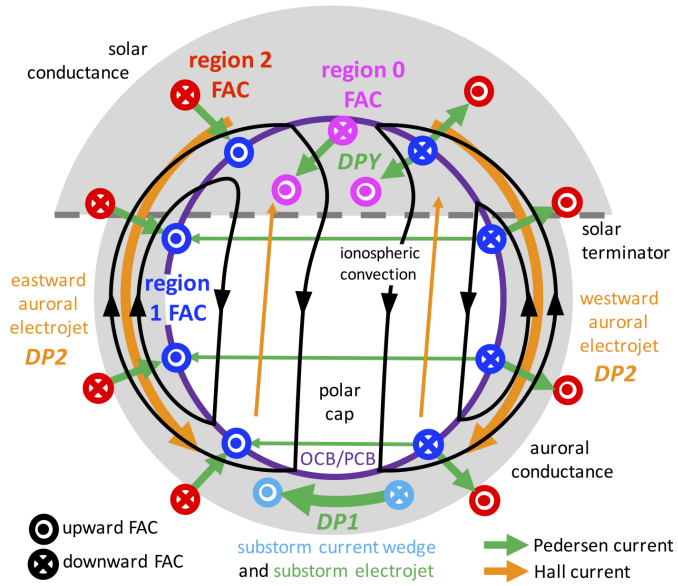

Figure 4: (Reproduced from *Milan et al.* [2017] under the Creative Commons Attribution 4.0 International License (http://creativecommons.org/licenses/by/4.0/)): A schematic of the ionospheric current systems in the northern polar region. The purple circle indicates the open/closed field line boundary (OCB). Black arrows denote streamlines of the typical ionospheric plasma flow. Region 1 FACs (blue) are coincident with the OCB at the poleward edge of the auroral zone, while the Region 2 FACs (red) are near the equatorward edge of the auroral zone. Region 0 FACs (magenta) flow in the cusp throat of the convection pattern (see *Milan et al.* [2017] for further details). Pedersen currents (green) flow horizontally between upwards and downwards FACs where the conductance is high (grey shading), and to a lesser degree across the polar cap where the conductance is low (no shading / white). The ionospheric electric field points in the same, or similar, direction as the Pedersen currents. Hall currents in the high conductance auroral zones form the eastward and westward auroral electrojets; weaker Hall currents flow sunwards across the polar cap. Substorm current wedge FACs (cyan) and the interconnecting substorm electrojet are present during substorm intervals, producing DP1 pattern magnetic perturbations. DPY perturbations are associated with closure of the region 0 FACs. DP2 perturbations are produced by the auroral electrojet-related currents.

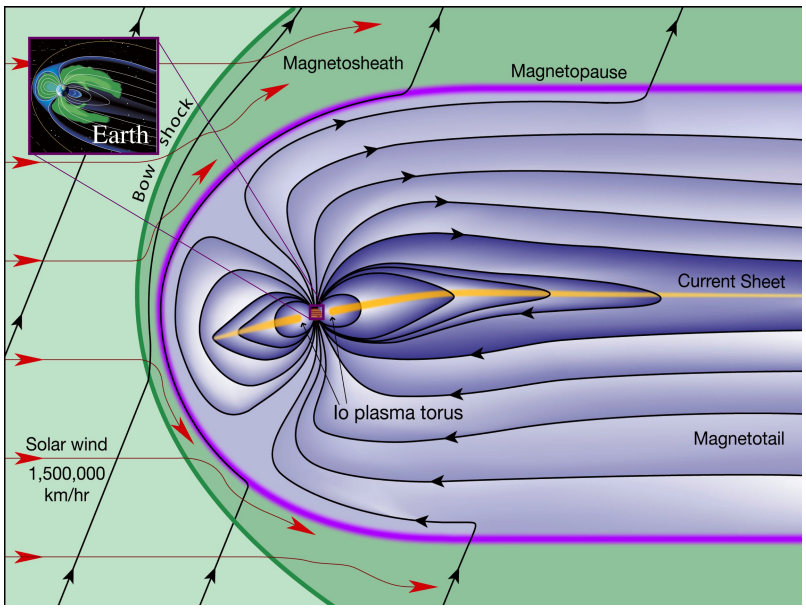

Figure 5: (Image Credit: Bagenal/Bartlett) Schematic diagram of Jupiter's magnetosphere in noon-midnight plane. Black arrowed curves indicate magnetic field lines. Yellow shaded region is the plasma sheet / current sheet. The inset shows Earth's dayside magnetosphere on a similar scale for comparison.

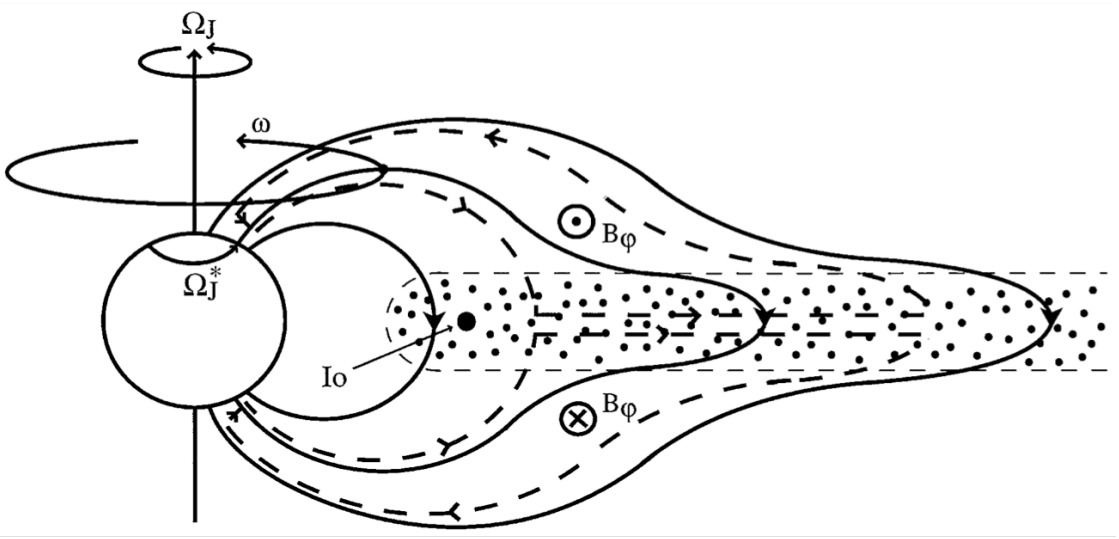

Figure 6: (From *Cowley and Bunce* [2001], reproduced by permission from Elsevier): Meridian cross-section through the Jovian magnetosphere. Arrowed solid lines indicate magnetic field lines, which are distended outwards in the middle magnetosphere by azimuthal currents in the plasma sheet. The plasma sheet plasma originates mainly at Io, which orbits at $\sim 6\mathrm{R_J}$ and releases of the order $\sim 10^3 \mathrm{kg\,s^{-1}}$ of sulphur / oxygen plasma (dotted region). Angular velocities are indicated by respective symbols Ω_J, Ω and Ω_J^* for the planet, a particular shell of field lines, and the neutral upper atmosphere (coexisting with the Pedersen conducting layer of the ionosphere). The coupling current system is schematically indicated by the arrowed dashed lines, shown here for the case of steady-state subcorotation of the plasma (i.e. $\Omega \leq \Omega_J$, as in the model of *Hill* [1979]). This current system bends field lines out of meridian planes, producing azimuthal field components B_φ.

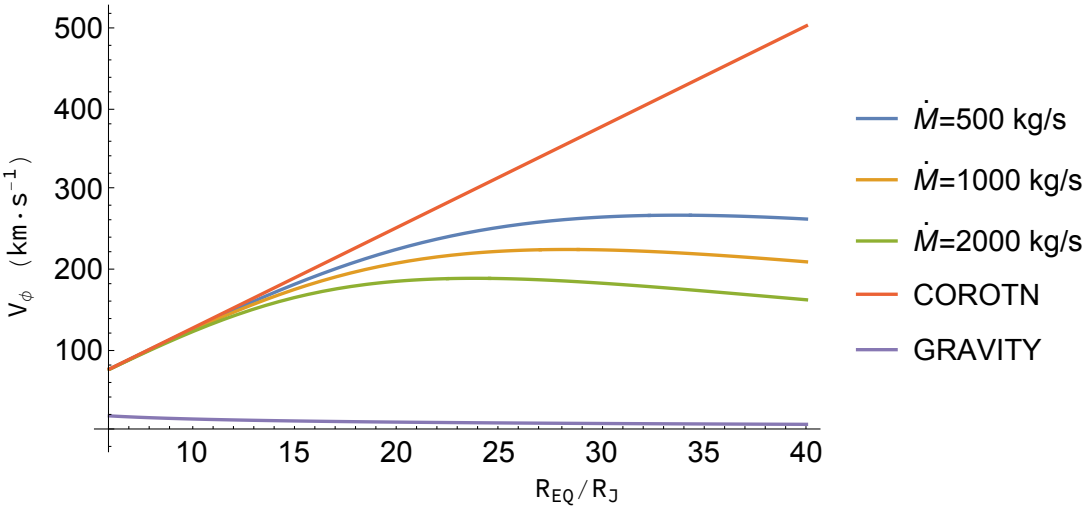

Figure 7: Solutions for azimuthal plasma velocity in the equatorial plane, calculated using the theory of *Hill* [1979] for an axisymmetric rotating magnetosphere with a pure dipole field of magnetic moment appropriate for Jupiter. Solutions are shown in units of $\mathrm{km} \cdot \mathrm{s}^{-1}$, as a function of equatorial radial distance in units of Jupiter radii. Curves are colour-coded according to the Iogenic plasma mass loading rate $\dot{M}$, and corotation and Keplerian rotation curves are also shown for comparison.

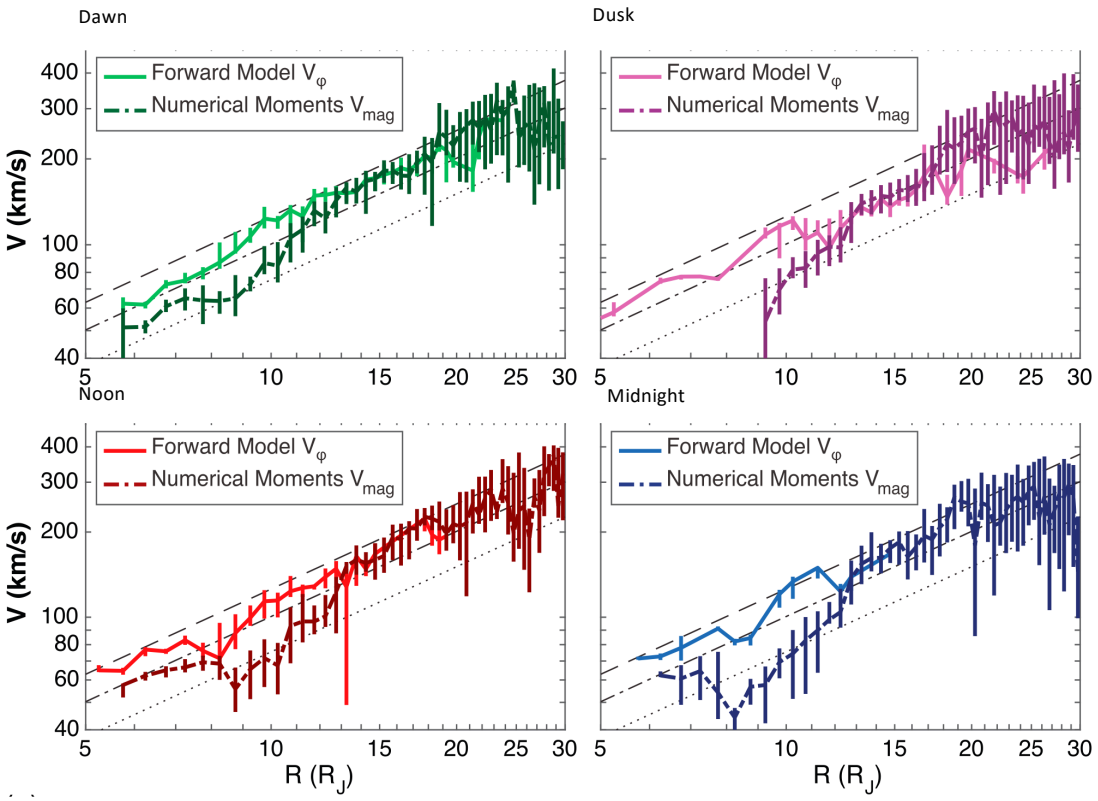

Figure 8: Observations of azimuthal plasma velocity near the Jovian equatorial plane, obtained through analysis of *Galileo* PLS (Plasma Science instrument) data by *Bagenal et al.* [2016]. Data are grouped according to local time sector indicated in the panel titles. PLS data were analyzed using the method of numerical moments (dark-coloured data points and dashed lines) to derive magnitude of the flow in spacecraft coordinates, and forward modelling (light-coloured data points and solid lines) for azimuthal components of flow in planet-centred spherical coordinates, referenced to Jupiter's rotation axis. The dot/dashed black lines show 100%, 80% and 60% of corotation. This figure was derived by extracting only the panels pertaining to plasma azimuthal velocity from the original figure in *Bagenal et al.* [2016].

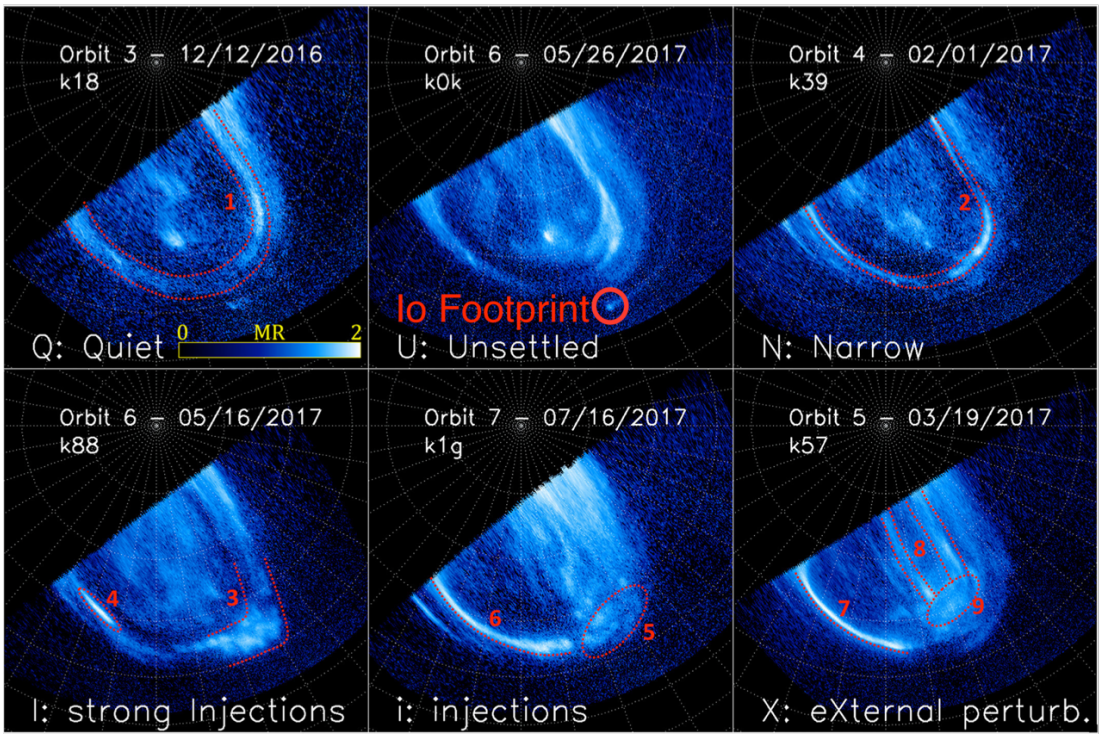

Figure 9: (Figure from *Grodent et al.* [2018], to which the reader is referred for further detail): Ultraviolet auroral images of Jupiter's northern hemisphere acquired with the Hubble Space Telescope Imaging Spectrograph (STIS) UV camera, and projected on a polar map with 10° spacing in latitude and longitude. The logarithmic blue shades colour bar in the upper left panel indicates the intensity of emission. Each auroral family (Q, U, N, J, I, i and X) displayed in the corresponding panel is potentially representative of a certain state of the magnetosphere. Auroral features characterising different morphologies are highlighted with red dashed lines, and ellipses and red numbers from '1' through '9'. For example, the parallel loci labelled '1' and '2' are the boundaries of the main emission (main oval, linked to corotation breakdown of the magnetodisc plasma) in its quiescent and narrowed states; the corner-shaped feature marked '3' in the lower left panel is typical of the strong injections (I) family. We have additionally highlighted the Io auroral footprint in the panel labelled 'U: unsettled'.

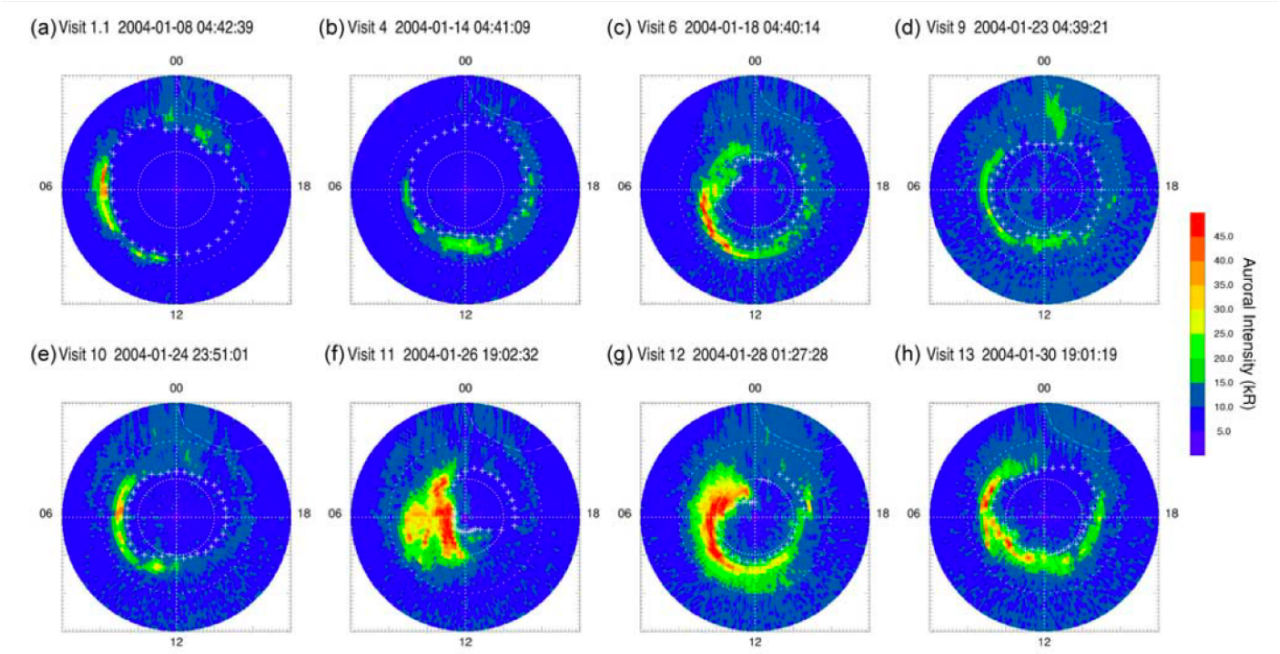

Figure 10: (From *Badman et al.* [2005], to which the reader is referred for further detail): Selection of UV images of Saturn's southern aurora taken during January 2004, with the visit number, date, and start time of each image shown at the top of each plot. The images are projected onto a polar grid, from the pole to 30° co-latitude, viewed as though looking 'through' the planet onto the southern pole. Noon is at the bottom of each plot, and dawn to the left. The UV auroral intensity is plotted according to the colour scale shown on the right-hand side. White crosses mark the poleward edge of the observed auroral features. Dashed white line in the pre-midnight sector marks a region of nightside emission attributed to solar UV photons scattered from Saturn's rings. The intensities shown are the average of two unfiltered images obtained over each HST orbit.

References

Achilleos, N., S. Miller, R. Prangé, G. Millward, and M. K. Dougherty, A dynamical model of Jupiter's auroral electrojet, *New J. Phys.*, *3*, 3–+, doi:10.1088/1367-2630/3/1/303, 2001.

Achilleos, N., N. André, X. Blanco-Cano, P. C. Brandt, P. A. Delamere, and R. Winglee, 1. Transport of Mass, Momentum and Energy in Planetary Magnetodisc Regions, *Space Sci. Rev.*, *187*, 229–299, doi:10.1007/s11214-014-0086-y, 2015.

Acuña, M. H., F. M. Neubauer, and N. F. Ness, Standing alfvén wave current system at io: Voyager 1 observations, *Journal of Geophysical Research: Space Physics*, *86*(A10), 8513–8521, doi:10.1029/JA086iA10p08513, 1981.

Akasofu, S. I., The development of the auroral substorm, *Planet. Space Sci.*, *12*(4), 273–282, doi:10.1016/0032-0633(64)90151-5, 1964.

Akasofu, S.-I., and S. Chapman, The development of the main phase of magnetic storms, *Journal of Geophysical Research (1896-1977)*, *68*(1), 125–129, doi:https://doi.org/10.1029/JZ068i001p00125, 1963.

Akasofu, S. I., and A. L. Snyder, Comments on the growth phase of magnetospheric substorms, *J. Geophys. Res.*, *77*(31), 6275, doi:10.1029/JA077i031p06275, 1972.

Andrews, D. J., S. W. H. Cowley, M. K. Dougherty, L. Lamy, G. Provan, and D. J. Southwood, Planetary period oscillations in Saturn's magnetosphere: Evolution of magnetic oscillation

properties from southern summer to post-equinox, *Journal of Geophysical Research (Space Physics)*, *117*, A04224, doi:10.1029/2011JA017444, 2012.

Bader, A., S. W. H. Cowley, S. V. Badman, L. C. Ray, J. Kinrade, B. Palmaerts, and W. R. Pryor, The morphology of saturn's aurorae observed during the cassini grand finale, *Geophysical Research Letters*, *47*(2), e2019GL085,800, doi:10.1029/2019GL085800, e2019GL085800 10.1029/2019GL085800, 2020.

Bader, A., et al., The dynamics of saturn's main aurorae, *Geophysical Research Letters*, *46*(17-18), 10,283–10,294, doi:10.1029/2019GL084620, 2019.

Badman, S. V., E. J. Bunce, J. T. Clarke, S. W. H. Cowley, J.-C. Gérard, D. Grodent, and S. E. Milan, Open flux estimates in saturn's magnetosphere during the january 2004 cassini-hst campaign, and implications for reconnection rates, *Journal of Geophysical Research: Space Physics*, *110*(A11), doi:10.1029/2005JA011240, 2005.

Badman, S. V., S. W. H. Cowley, L. Lamy, B. Cecconi, and P. Zarka, Relationship between solar wind corotating interaction regions and the phasing and intensity of saturn kilometric radiation bursts, *Annales Geophysicae*, *26*(12), 3641–3651, doi:10.5194/angeo-26-3641-2008, 2008.

Bagenal, F., and P. A. Delamere, Flow of mass and energy in the magnetospheres of Jupiter and Saturn, *J. Geophys. Res.*, *116*, A05209, doi:10.1029/2010JA016294, 2011.

Bagenal, F., R. J. Wilson, S. Siler, W. R. Paterson, and W. S. Kurth, Survey of galileo plasma observations in jupiter's plasma sheet, *Journal of Geophysical Research: Planets*, *121*(5), 871–894, doi:10.1002/2016JE005009, 2016.

Baker, D. N., T. A. Fritz, R. L. McPherron, D. H. Fairfield, Y. Kamide, and W. Baumjohann, Magnetotail energy storage and release during the cdaw 6 substorm analysis intervals, *Journal of Geophysical Research: Space Physics*, *90*(A2), 1205–1216, doi:https://doi.org/10.1029/JA090iA02p01205, 1985.

Baker, D. N., R. C. Anderson, R. D. Zwickl, and J. A. Slavin, Average plasma and magnetic field variations in the distant magnetotail associated with near-earth substorm effects, *Journal of Geophysical Research: Space Physics*, *92*(A1), 71–81, doi:https://doi.org/10.1029/JA092iA01p00071, 1987.

Belcher, J. W., The Jupiter-Io Connection: An Alfven Engine in Space, *Science*, *238*(4824), 170–176, doi:10.1126/science.238.4824.170, 1987.

Birkeland, K. R., The Norwegian auroral Polaris Expedition. 1902-1903., 1918.

Bonfond, B., *When Moons Create Aurora: The Satellite Footprints on Giant Planets*, pp. 133–140, American Geophysical Union (AGU), doi:10.1029/2011GM001169, 2013.

Bougher, S. W., R. G. Roble, and T. Fuller-Rowell, *Simulations of the Upper Atmospheres of the Terrestrial Planets*, pp. 261–288, American Geophysical Union (AGU), doi:https://doi.org/10.1029/130GM17, 2002.

Bunce, E. J., *Origins of Saturn's Auroral Emissions and their Relationship to Large-Scale Magnetosphere Dynamics*, pp. 397–410, American Geophysical Union (AGU), doi:10.1029/2011GM001191, 2013.

Cao, H., C. T. Russell, U. R. Christensen, M. K. Dougherty, and M. E. Burton, Saturn's very axisymmetric magnetic field: No detectable secular variation or tilt, *Earth and Planetary Science Letters*, *304*, 22–28, doi:10.1016/j.epsl.2011.02.035, 2011.

Carbary, J. F., and D. G. Mitchell, Periodicities in Saturn's magnetosphere, *Reviews of Geophysics*, *51*, 1–30, doi:10.1002/rog.20006, 2013.

Carbary, J. F., D. G. Mitchell, S. M. Krimigis, D. C. Hamilton, and N. Krupp, Charged particle periodicities in Saturn's outer magnetosphere, *J. Geophys. Res.*, *112*, A06246, doi:10.1029/2007JA012351, 2007.

Carbary, J. F., D. G. Mitchell, P. Brandt, C. Paranicas, and S. M. Krimigis, ENA periodicities at Saturn, *Geophys. Res. Lett.*, *35*, L07102, doi:10.1029/2008GL033230, 2008.

Chapman, S., Magnetic storms, The energy of, *Mon. Not. Royal Ast. Soc.*, *79*, 70, doi:10.1093/mnras/79.1.70, 1918.

Clarke, J. T., *Auroral Processes on Jupiter and Saturn*, pp. 113–122, American Geophysical Union (AGU), doi:10.1029/2011GM001199, 2013.

Clarke, J. T., et al., Ultraviolet emissions from the magnetic footprints of Io, Ganymede and Europa on Jupiter, *Nature*, *415*(6875), 997–1000, 2002.

Clarke, K. E., D. J. Andrews, C. S. Arridge, A. J. Coates, and S. W. H. Cowley, Magnetopause oscillations near the planetary period at Saturn: Occurrence, phase, and amplitude, *Journal of Geophysical Research (Space Physics)*, *115*, A08209, doi:10.1029/2009JA014745, 2010.

Cowley, S. W. H., and E. J. Bunce, Origin of the main auroral oval in Jupiter's coupled magnetosphere-ionosphere system, *Planet. Space Sci.*, *49*, 1067–1088, doi:10.1016/S0032-0633(00)00167-7, 2001.

Cowley, S. W. H., and G. Provan, Planetary period modulations of Saturn's magnetotail current sheet during northern spring: Observations and modeling, *Journal of Geophysical Research (Space Physics)*, *122*(6), 6049–6077, 2017.

Cowley, S. W. H., E. J. Bunce, T. S. Stallard, and S. Miller, Jupiter's polar ionospheric flows: Theoretical interpretation, *Geophysical Research Letters*, *30*(5), doi:10.1029/2002GL016030, 2003.

Cowley, S. W. H., E. J. Bunce, and J. M. O'Rourke, A simple quantitative model of plasma flows and currents in Saturn's polar ionosphere, *Journal of Geophysical Research (Space Physics)*, *109*(A5), A05212, doi:10.1029/2003JA010375, 2004.

Cowley, S. W. H., J. D. Nichols, and D. J. Andrews, Modulation of Jupiter's plasma flow, polar currents, and auroral precipitation by solar wind-induced compressions and expansions of the magnetosphere: a simple theoretical model, *Ann. Geophys.*, *25*, 1433–1463, doi:10.5194/angeo-25-1433-2007, 2007.

Cowley, S. W. H., et al., Auroral current systems in saturn's magnetosphere: comparison of theoretical models with cassini and hst observations, *Annales Geophysicae*, *26*(9), 2613–2630, doi:10.5194/angeo-26-2613-2008, 2008.

Desch, M. D., and M. L. Kaiser, Voyager measurement of the rotation period of Saturn's magnetic field, *Geophys. Res. Lett.*, *8*, 253–256, doi:10.1029/GL008i003p00253, 1981.

Desroche, M., F. Bagenal, P. A. Delamere, and N. Erkaev, Conditions at the expanded jovian magnetopause and implications for the solar wind interaction, *Journal of Geophysical Research: Space Physics*, *117*(A7), doi:10.1029/2012JA017621, 2012.

Dungey, J. W., Interplanetary magnetic field and the auroral zones, *Phys. Rev. Lett.*, *6*, 47–48, doi:10.1103/PhysRevLett.6.47, 1961.

Ergun, R. E., C. W. Carlson, J. P. McFadden, G. T. Delory, R. J. Strangeway, and P. L. Pritchett, Electron-Cyclotron Maser Driven by Charged-Particle Acceleration from Magnetic Field-aligned Electric Fields, *Astrophysical Journal*, *538*(1), 456–466, doi:10.1086/309094, 2000.

Espinosa, S. A., and M. K. Dougherty, Periodic perturbations in Saturn's magnetic field, *Geophys. Res. Lett.*, *27*, 2785–2788, doi:10.1029/2000GL000048, 2000.

Ferrière, K. M., and N. André, A mixed magnetohydrodynamic-kinetic theory of low-frequency waves and instabilities in stratified, gyrotropic, two-component plasmas, *Journal of Geophysical Research (Space Physics)*, *108*, 1308, doi:10.1029/2003JA009883, 2003.

Ferrière, K. M., C. Zimmer, and M. Blanc, Magnetohydrodynamic waves and gravitational/centrifugal instability in rotating systems, *J. Geophys. Res.*, *104*, 17,335–17,356, doi:10.1029/1999JA900167, 1999.

Frey, H. U., S. B. Mende, V. Angelopoulos, and E. F. Donovan, Substorm onset observations

by IMAGE-FUV, *Journal of Geophysical Research (Space Physics)*, *109*(A10), A10304, doi: 10.1029/2004JA010607, 2004.

Galand, M., and S. Chakrabarti, *Auroral Processes in the Solar System*, pp. 55–76, American Geophysical Union (AGU), doi:https://doi.org/10.1029/130GM05, 2002.

Giampieri, G., M. K. Dougherty, E. J. Smith, and C. T. Russell, A regular period for Saturn's magnetic field that may track its internal rotation, *NATURE*, *441*, 62–64, doi: 10.1038/nature04750, 2006.

Gladstone, G. R., R. V. Yelle, and T. Majeed, *Solar System Upper Atmospheres: Photochemistry, Energetics, and Dynamics*, pp. 23–37, American Geophysical Union (AGU), doi: https://doi.org/10.1029/130GM03, 2002.

Gold, T., Motions in the magnetosphere of the earth, *J. Geophys. Res.*, *64*, 1219–1224, 1959.

Goldreich, P., and D. Lynden-Bell, Io, a jovian unipolar inductor, *Astrophysical Journal*, *156*, 59–78, doi:10.1086/149947, 1969.

Grodent, D., A. Radioti, B. Bonfond, and J.-C. Gérard, On the origin of saturn's outer auroral emission, *Journal of Geophysical Research: Space Physics*, *115*(A8), doi: 10.1029/2009JA014901, 2010.

Grodent, D., et al., Jupiter's aurora observed with hst during juno orbits 3 to 7, *Journal of Geophysical Research: Space Physics*, *123*(5), 3299–3319, doi:10.1002/2017JA025046, 2018.

Gurnett, D. A., A. M. Persoon, W. S. Kurth, J. B. Groene, T. F. Averkamp, M. K. Dougherty,

and D. J. Southwood, The variable rotation period of the inner region of saturn's plasma disk, *Science*, *316*(5823), 442–445, doi:10.1126/science.1138562, 2007.

Gurnett, D. A., A. M. Persoon, J. B. Groene, A. J. Kopf, G. B. Hospodarsky, and W. S. Kurth, A north-south difference in the rotation rate of auroral hiss at Saturn: Comparison to Saturn's kilometric radio emission, *Geophys. Res. Lett.*, *36*, L21108, doi:10.1029/2009GL040774, 2009.

Gurnett, D. A., et al., Radio and Plasma Wave Observations at Saturn from Cassini's Approach and First Orbit, *Science*, *307*, 1255–1259, doi:10.1126/science.1105356, 2005.

Hargreaves, J. K., *Frontmatter*, pp. i–vi, Cambridge Atmospheric and Space Science Series, Cambridge University Press, 1992.

Hill, T. W., Interchange stability of a rapidly rotating magnetosphere, *Planet. Space Sci.*, *24*, 1151–1154, 1976.

Hill, T. W., Inertial limit on corotation, *J. Geophys. Res.*, *84*, 6554–6558, doi: 10.1029/JA084iA11p06554, 1979.

Hill, T. W., et al., Plasmoids in Saturn's magnetotail, *J. Geophys. Res.*, *113*, A01214, doi: 10.1029/2007JA012626, 2008.

Hones Jr., E. W., Magnetic reconnection in space and laboratory plasmas, *Eos, Transactions American Geophysical Union*, *65*(18), 340–341, doi: https://doi.org/10.1029/EO065i018p00340, 1984.

Hunt, G. J., G. Provan, E. J. Bunce, S. W. H. Cowley, M. K. Dougherty, and D. J. Southwood, Field-Aligned Currents in Saturn's Magnetosphere: Observations From the F-Ring Orbits, *Journal of Geophysical Research (Space Physics)*, *123*(5), 3806–3821, doi: 10.1029/2017JA025067, 2018.

Hunt, G. J., E. J. Bunce, H. Cao, S. W. H. Cowley, M. K. Dougherty, G. Provan, and D. J. Southwood, Saturn's Auroral Field-Aligned Currents: Observations From the Northern Hemisphere Dawn Sector During Cassini's Proximal Orbits, *Journal of Geophysical Research (Space Physics)*, *125*(5), e27683, doi:10.1029/2019JA027683, 2020.

Ioannidis, G., and N. Brice, Plasma densities in the jovian magnetosphere: Plasma slingshot or maxwell demon?, *Icarus*, *14*(3), 360–373, doi:https://doi.org/10.1016/0019-1035(71)90007-8, 1971.

Jackman, C. M., C. T. Russell, et al., Strong rapid dipolarizations in saturn's magnetotail..., *Geophys. Res. Lett.*, *34*, L11,203, 2007.

Jia, X., M. G. Kivelson, and T. I. Gombosi, Driving Saturn's magnetospheric periodicities from the upper atmosphere/ionosphere, *Journal of Geophysical Research (Space Physics)*, *117*(A4), A04215, doi:10.1029/2011JA017367, 2012.

Kivelson, M. G., and D. J. Southwood, Dynamical consequences of two modes of centrifugal instability in Jupiter's outer magnetosphere, *J. Geophys. Res.*, *110*, A12,209, 2005.

Knight, S., Parallel electric fields, *Planetary and Space Science*, *21*(5), 741 – 750, doi: https://doi.org/10.1016/0032-0633(73)90093-7, 1973.

Kurth, W. S., T. F. Averkamp, et al., An update to a Saturnian longitude system based on kilometric radio emissions, *J. Geophys. Res.*, *113*, A05,222, 2008.

Kurth, W. S., et al., A new view of jupiter's auroral radio spectrum, *Geophysical Research Letters*, *44*(14), 7114–7121, doi:10.1002/2017GL072889, 2017.

Lamy, L., R. Prangé, W. Pryor, J. Gustin, S. V. Badman, H. Melin, T. Stallard, D. Mitchell, and P. C. Brandt, Multispectral simultaneous diagnosis of saturn's aurorae throughout a planetary rotation, *Journal of Geophysical Research: Space Physics*, *118*(8), 4817–4843, doi:10.1002/jgra.50404, 2013.

Le Quéau, D., *Planetary radio emissions from high magnetic latitudes: The 'cyclotron maser' theory, from 'Planetary Radio Emissions II' (ed. H. O. Rucker, M. L. Kaiser, and Y. Leblanc)*, pp. 381–398, Austrian Academy of Sciences, 1988.

Liou, K., P. T. Newell, C. I. Meng, A. T. Y. Lui, M. Brittnacher, and G. Parks, Dayside auroral activity as a possible precursor of substorm onsets: A survey using Polar ultraviolet imagery, *J. Geophys. Res.*, *102*(A9), 19,835–19,844, doi:10.1029/97JA01741, 1997.

Lysak, R. L., and Y. Song, Nonlocal kinetic theory of alfvén waves on dipolar field lines, *Journal of Geophysical Research: Space Physics*, *108*(A8), doi:10.1029/2003JA009859, 2003.

Masters, A., Model-based assessments of magnetic reconnection and kelvin-helmholtz instability at jupiter's magnetopause, *Journal of Geophysical Research: Space Physics*, *122*(11), 11,154–11,174, doi:10.1002/2017JA024736, 2017.

Mauk, B. H., et al., Diverse electron and ion acceleration characteristics observed over jupiter's main aurora, *Geophysical Research Letters*, *45*(3), 1277–1285, doi:10.1002/2017GL076901, 2018.

McComas, D. J., and F. Bagenal, Jupiter: A fundamentally different magnetospheric interaction with the solar wind, *Geophysical Research Letters*, *34*(20), doi:10.1029/2007GL031078, 2007.

McPherron, R. L., Substorm related changes in the geomagnetic tail: The growth phase, *Planet. Space Sci.*, *20*(9), 1521–1539, doi:10.1016/0032-0633(72)90054-2, 1972.

McPherron, R. L., C. T. Russell, and M. P. Aubry, Satellite studies of magnetospheric substorms on August 15, 1968: 9. Phenomenological model for substorms, *J. Geophys. Res.*, *78*(16), 3131, doi:10.1029/JA078i016p03131, 1973.

Melrose, D., Rotational effects on the distribution of thermal plasma in the magnetosphere of jupiter, *Planetary and Space Science*, *15*(2), 381–393, doi:https://doi.org/10.1016/0032-0633(67)90202-4, 1967.

Melrose, D. B., and G. A. Dulk, Electron-cyclotron masers as the source of certain solar and stellar radio bursts., *Astrophysical Journal*, *259*, 844–858, doi:10.1086/160219, 1982.

Milan, S. E., et al., Overview of Solar Wind-Magnetosphere-Ionosphere-Atmosphere Coupling and the Generation of Magnetospheric Currents, *SSR*, *206*(1-4), 547–573, doi:10.1007/s11214-017-0333-0, 2017.

Millward, G., S. Miller, A. Aylward, I. Müller-Wodard, and N. Achilleos, *Thermospheric General Circulation Models for the Giant Planets: The Jupiter Case*, pp. 289–298, American Geophysical Union (AGU), doi:https://doi.org/10.1029/130GM18, 2002.

Moos, N. A. F., Magnetic Observations Made at the Government Observatory, Bombay, for the Period 1846 to 1905 and Their Discussion, part II, The Phenomenon and Its Discussion, *"Bombay Observatory"*, 1910.

Nagy, A. F., and T. E. Cravens, *Solar System Ionospheres*, pp. 39–54, American Geophysical Union (AGU), doi:https://doi.org/10.1029/130GM04, 2002.

Newell, P. T., A. R. Lee, K. Liou, S.-I. Ohtani, T. Sotirelis, and S. Wing, Substorm cycle dependence of various types of aurora, *Journal of Geophysical Research: Space Physics*, *115*(A9), doi:https://doi.org/10.1029/2010JA015331, 2010.

Nichols, J., and S. Cowley, Magnetosphere-ionosphere coupling currents in Jupiter's middle magnetosphere: effect of precipitation-induced enhancement of the ionospheric Pedersen conductivity, *Ann. Geophys.*, *22*, 1799–1827, doi:10.5194/angeo-22-1799-2004, 2004.

Nichols, J. D., J. T. Clarke, S. W. H. Cowley, J. Duval, A. J. Farmer, J.-C. Gérard, D. Grodent, and S. Wannawichian, Oscillation of saturn's southern auroral oval, *Journal of Geophysical Research: Space Physics*, *113*(A11), doi:10.1029/2008JA013444, 2008.

Olsson, A., P. Janhunen, T. Karlsson, N. Ivchenko, and L. G. Blomberg, Statistics of joule heating in the auroral zone and polar cap using astrid-2 satellite poynting flux, *Annales Geophysicae*, *22*(12), 4133–4142, doi:10.5194/angeo-22-4133-2004, 2004.

Paranicas, C., D. G. Mitchell, E. C. Roelof, P. C. Brandt, D. J. Williams, S. M. Krimigis, and B. H. Mauk, Periodic intensity variations in global ENA images of Saturn, *Geophys. Res. Lett.*, *32*, L21101, doi:10.1029/2005GL023656, 2005.

Piddington, J. H., and J. F. Drake, Electrodynamic Effects of Jupiter's Satellite Io, *Nature*, *217*, 935–937, doi:10.1038/217935a0, 1968.

Prangé, R., D. Rego, D. Southwood, P. Zarka, S. Miller, and W. Ip, Rapid energy dissipation and variability of the lo-Jupiter electrodynamic circuit, *Nature*, *379*(6563), 323–325, doi:10.1038/379323a0, 1996.

Queinnec, J., and P. Zarka, Io-controlled decameter arcs and io-jupiter interaction, *Journal of Geophysical Research: Space Physics*, *103*(A11), 26,649–26,666, doi:10.1029/98JA02435, 1998.

Ramer, K. M., M. G. Kivelson, N. Sergis, K. K. Khurana, and X. Jia, Spinning, breathing, and flapping: Periodicities in Saturn's middle magnetosphere, *Journal of Geophysical Research (Space Physics)*, *122*(1), 393–416, doi:10.1002/2016JA023126, 2017.

Ray, L. C., Y.-J. Su, R. E. Ergun, P. A. Delamere, and F. Bagenal, Current-voltage relation of a centrifugally confined plasma, *Journal of Geophysical Research: Space Physics*, *114*(A4), doi:10.1029/2008JA013969, 2009.

Ray, L. C., R. E. Ergun, P. A. Delamere, and F. Bagenal, Magnetosphere-ionosphere coupling at jupiter: Effect of field-aligned potentials on angular momentum transport, *Journal of Geophysical Research: Space Physics*, *115*(A9), doi:10.1029/2010JA015423, 2010.

Ray, L. C., N. A. Achilleos, and J. N. Yates, The effect of including field-aligned potentials in the coupling between jupiter's thermosphere, ionosphere, and magnetosphere, *Journal of Geophysical Research: Space Physics*, *120*(8), 6987–7005, doi:10.1002/2015JA021319, 2015.

Rishbeth, H., and O. K. Garriott, *Introduction to ionospheric physics*, x, 331 p. pp., Academic Press New York, 1969.

Rostoker, G., The evolving concept of a magnetospheric substorm, *Journal of Atmospheric and Solar-Terrestrial Physics*, *61*(1), 85–100, doi:https://doi.org/10.1016/S1364-6826(98)00119-9, 1999.

Satoh, T., and J. E. P. Connerney, Jupiter's H $^{+}_{3}$ Emissions Viewed in Corrected Jovimagnetic Coordinates, *Icarus*, *141*(2), 236–252, doi:10.1006/icar.1999.6173, 1999.

Saur, J., et al., Wave-particle interaction of alfvén waves in jupiter's magnetosphere: Auroral and magnetospheric particle acceleration, *Journal of Geophysical Research: Space Physics*, *123*(11), 9560–9573, doi:10.1029/2018JA025948, 2018.

Schunk, R., *Ionospheric Models for Earth*, pp. 299–306, American Geophysical Union (AGU), doi:https://doi.org/10.1029/130GM19, 2002.

Scudder, J. D., E. C. Sittler, and H. S. Bridge, A survey of the plasma electron environment of Jupiter - A view from Voyager, *J. Geophys. Res.*, *86*, 8157–8179, doi:10.1029/JA086iA10p08157, 1981.

Smith, C. G. A., and N. Achilleos, Axial symmetry breaking of Saturn's thermosphere, *Mon. Not. Royal Ast. Soc.*, *422*, 1460–1488, doi:10.1111/j.1365-2966.2012.20719.x, 2012.

Smith, C. G. A., and A. D. Aylward, Coupled rotational dynamics of Jupiter's thermosphere and magnetosphere, *Ann. Geophys.*, *27*, 199–230, 2009.

Smith, C. G. A., L. C. Ray, and N. A. Achilleos, A planetary wave model for Saturn's 10.7-h periodicities, *Icarus*, *268*, 76–88, doi:10.1016/j.icarus.2015.12.041, 2016.

Sorba, A. M., N. A. Achilleos, P. Guio, C. S. Arridge, N. Sergis, and M. K. Dougherty, The Periodic Flapping and Breathing of Saturn's Magnetodisk During Equinox, *Journal of Geophysical Research (Space Physics)*, *123*(10), 8292–8316, doi:10.1029/2018JA025764, 2018.

Southwood, D. J., and E. Chané, High-latitude circulation in giant planet magnetospheres, *Journal of Geophysical Research: Space Physics*, *121*(6), 5394–5403, doi:10.1002/2015JA022310, 2016.

Southwood, D. J., and S. W. H. Cowley, The origin of Saturn's magnetic periodicities: Northern and southern current systems, *Journal of Geophysical Research (Space Physics)*, *119*(3), 1563–1571, doi:10.1002/2013JA019632, 2014.

Southwood, D. J., and M. G. Kivelson, Magnetospheric interchange instability, *J. Geophys. Res.*, *92*, 109–116, doi:10.1029/JA092iA01p00109, 1987.

Stallard, T., S. Miller, H. Melin, M. Lystrup, S. W. H. Cowley, E. J. Bunce, N. Achilleos, and M. Dougherty, Jovian-like aurorae on Saturn, *Nature*, *453*(7198), 1083–1085, doi:10.1038/nature07077, 2008.

Stallard, T. S., S. Miller, L. M. Trafton, T. R. Geballe, and R. D. Joseph, Ion

winds in saturn's southern auroral/polar region, *Icarus*, *167*(1), 204 – 211, doi: https://doi.org/10.1016/j.icarus.2003.09.006, special Issue on DS1/Comet Borrelly, 2004.

Thomsen, M. F., C. M. Jackman, S. W. H. Cowley, X. Jia, M. G. Kivelson, and G. Provan, Evidence for periodic variations in the thickness of Saturn's nightside plasma sheet, *Journal of Geophysical Research (Space Physics)*, *122*(1), 280–292, doi:10.1002/2016JA023368, 2017.

Thorne, R. M., Radiation belt dynamics: The importance of wave-particle interactions, *Geophys. Res. Lett.*, *37*, L22107, doi:10.1029/2010GL044990, 2010.

Vasyliūnas, V. M., Plasma distribution and flow, in *Physics of the Jovian Magnetosphere*, edited by A. J. Dessler, pp. 395–453, Cambridge University Press, New York, iSBN 0521520061 (paperback), 1983.

Waite Jr., J. H., and D. Lummerzheim, *Comparison of Auroral Processes: Earth and Jupiter*, pp. 115–139, American Geophysical Union (AGU), doi:https://doi.org/10.1029/130GM08, 2002.

Weimer, D. R., J. R. Kan, and S. I. Akasofu, Variations of the Polar Cap Potential Measured During Magnetospheric Substorms, *J. Geophys. Res.*, *97*(A4), 3945–3951, doi: 10.1029/91JA03159, 1992.

Wing, S., M. Gkioulidou, J. R. Johnson, P. T. Newell, and C.-P. Wang, Auroral particle precipitation characterized by the substorm cycle, *Journal of Geophysical Research (Space Physics)*, *118*(3), 1022–1039, doi:10.1002/jgra.50160, 2013.

Wu, C. S., and L. C. Lee, A theory of the terrestrial kilometric radiation., *Astrophysical Journal*, *230*, 621–626, doi:10.1086/157120, 1979.

Yates, J. N., N. Achilleos, and P. Guio, Influence of upstream solar wind on thermospheric flows at Jupiter, *Planet. Space Sci.*, *61*, 15–31, doi:10.1016/j.pss.2011.08.007, 2012.

Yates, J. N., L. C. Ray, and N. Achilleos, An initial study into the long-term influence of solar wind dynamic pressure on jupiter's thermosphere, *Journal of Geophysical Research: Space Physics*, *123*(11), 9357–9369, doi:10.1029/2018JA025828, 2018.

Yates, J. N., L. C. Ray, N. Achilleos, O. Witasse, and N. Altobelli, Magnetosphere-Ionosphere-Thermosphere Coupling at Jupiter Using a Three-Dimensional Atmospheric General Circulation Model, *Journal of Geophysical Research (Space Physics)*, *125*(1), e26792, doi:10.1029/2019JA026792, 2020.

Zarka, P., Auroral radio emissions at the outer planets: Observations and theories, *Journal of Geophysical Research: Planets*, *103*(E9), 20,159–20,194, doi:10.1029/98JE01323, 1998.

Zarka, P., T. Farges, B. P. Ryabov, M. Abada-Simon, and L. Denis, A scenario for Jovian S-bursts, *Geophys. Res. Lett.*, *23*(2), 125–128, doi:10.1029/95GL03780, 1996.